# Emergence of Dip2-mediated Specific DAG-based PKC Signalling Axis in Eukaryotes

Sakshi Shambhavi[#1,3], Sudipta Mondal[#1], Arnab Chakraborty[2], Nikita Shukla[1], Bapin K. Panda[1], Santhosh Kumar[1,3], Priyadarshan Kinatukara[1], Biswajit Pal[1], Siddhesh S. Kamat[2] and Rajan Sankaranarayanan[1,3]*

[1]CSIR-Centre for Cellular and Molecular Biology, Hyderabad, India

[2]Department of Biology, Indian Institute of Science Education and Research (IISER), Pune, India

[3]Academy of Scientific and Innovative Research (AcSIR), Ghaziabad, India-201002

[#]These authors have contributed equally

*For correspondence: sankar@ccmb.res.in

**Abstract**

Diacylglycerols (DAGs) are used for metabolic purposes and are tightly regulated secondary lipid messengers in eukaryotes. DAG subspecies with different fatty-acyl chains are proposed to be involved in the activation of distinct PKC isoforms, resulting in diverse physiological outcomes. However, the molecular players and the regulatory origin for fine-tuning the PKC pathway are unknown. Here, we show that Dip2, a conserved DAG regulator across Fungi and Animalia, has emerged as a modulator of PKC signalling in yeast. Dip2 maintains the level of a specific DAG subpopulation, required for the activation of PKC-mediated cell wall integrity pathway. Interestingly, the canonical DAG-metabolism pathways, being promiscuous, are decoupled from PKC signalling. We demonstrate that these DAG subspecies are sourced from a phosphatidylinositol pool generated by the acyl-chain remodelling pathway. Furthermore, we provide insights into the intimate coevolutionary relationship between the regulator (Dip2) and the effector (PKC) of DAG-based signalling. Hence, our study underscores the establishment of Dip2-PKC axis about 1.2 billion years ago in Opisthokonta, which marks the rooting of the first specific DAG-based signalling module of eukaryotes.

**Keywords**: Cell wall integrity/ Coevolution/ Diacylglycerol/ Dip2/ Lipid metabolism/ PKC

## Introduction:

Diacylglycerol (DAG) is a conserved lipid molecule with well-established roles in membrane lipid biogenesis and storage lipid production in all life forms. DAGs are synthesized via *de novo* pathways of lipid metabolism utilising fatty acid precursors, while it can also be generated as a by-product of multiple salvage pathways in eukaryotes (Carrasco & Merida, 2007; Eichmann & Lass, 2015). DAGs are unique as they lack headgroups unlike the other abundant lipid classes. They exhibit diversity due to variations in acyl-chain length and unsaturation. These acyl-chain variations are proposed to be the basis for the multifaceted physiological roles of DAGs in metabolic and signal transduction pathways (Marignani et al, 1996; Milne et al, 2008; Schuhmacher et al, 2020). The signalling function is executed by various 'DAG effector' proteins such as DAG-dependent protein kinases, Chimaerin, Munc13, RasGRP etc. involved in cell-cycle progression, neurotransmitter release, actin cytoskeleton organization and malignant transformation (Colon-Gonzalez & Kazanietz, 2006; Yang & Kazanietz, 2003). Studies conducted ~four decades ago have indicated the role of acyl-chain compositions of DAGs in Protein Kinase C (PKC) activation (Kishimoto et al, 1980; Marignani et al., 1996; Mori et al, 1982, Kamiya et al., 2016; Masayoshi et al., 1987). However, the cellular pathways for such specific acyl-chain-based regulation of signalling events have not been identified till date.

PKC, a serine/threonine protein kinase, is a classic example of a eukaryotic DAG-based signalling molecule. Mammalian PKC isoforms play a key role in a myriad of biological processes like cell differentiation, cell migration, mitochondrial functioning, cell polarity, etc. (Newton, 2018) and its dysregulation is associated with various pathological conditions such as cancer, diabetes, Alzheimer's, heart disease, obesity and age-related metabolic disorders (Etcheberrigaray et al, 2004; Marrocco et al, 2019; Nishizuka, 1984; Schmitz-Peiffer & Biden, 2008). Fungi, on the other hand, harbour a single PKC gene (*PKC1*) that is implicated in regulating the cell wall biosynthesis pathway, rationalizing its essentiality under normal growth

conditions (Levin, 2005). Genetic or pharmacological impairment of Pkc1 in pathogenic fungi like *Candida albicans, Cryptococcus neoformans etc.,* confers hypersensitivity to various antifungal drugs and drastically attenuates its proliferation and virulence in murine model (Heinisch & Rodicio, 2018; LaFayette et al, 2010) suggesting a crucial role of Pkc1 in pathogenicity of diverse fungal groups. The array of pathologies and disrupted cellular processes owing to hampered Pkc1 signalling warrants the necessity of stringent regulation of Pkc1 activity.

Although DAG-based activation of PKC is well established in metazoans, the role of specific acyl-chain compositions in fungi is still a mystery. Additionally, the molecular players regulating these signalling DAGs remain underexplored. Recently, we have identified and functionally characterized a conserved protein family, Disco-Interacting Protein 2 (Dip2) (earlier annotated as Cmr2 in yeast; SGD ID: S000005619), harbouring two tandem fatty acyl-AMP ligase-like domains (FLD1 and FLD2) along with a DMAP-binding domain 1 (DBD1) at the N-terminus (Mondal et al, 2022). We showed that Dip2 regulates specific DAG subspecies in terms of its acyl chain length and unsaturation across fungi and animals. Dip2 from *Saccharomyces cerevisiae* has been shown to be involved in converting C36:0 (18:0/18:0) and C36:1 (18:0/18:1) DAGs to triacylglycerols (TAGs) with corresponding chain lengths. These DAG subspecies constitute only ~0.5 % of the total lipid pool but are important for maintaining the organellar and thereby cellular homeostasis. However, the necessity to introduce such strict regulation of specific DAG subspecies in Opisthokonta remains elusive.

Here, we show that Dip2 has emerged as a modulator of Pkc1 signalling in the model yeast *Saccharomyces cerevisiae* by regulating the chain-length specific DAGs. By combining genetic and lipidomic approaches, we have demonstrated that the absence of Dip2, which leads to the accumulation of C36:0 and C36:1 DAGs, results in hyperactivation of Pkc1. This in turn elevates the downstream signalling of cell wall integrity (CWI) pathway leading to cell wall

stress resistance. On the contrary, the bulk DAG pool, which is generally acted upon by canonical DAG metabolizing enzymes, fails to activate Pkc1. The DAG binding domain of Pkc1 displays a remarkable specificity to certain DAG subspecies *in vitro,* reflecting the *in vivo* specificity. To understand this metabolic segregation of DAG pool, we have tracked the source of the Dip2-metabolised DAG subspecies involved in Pkc1 activation. Interestingly, it was found to be channelled majorly through the phosphatidylinositol (PI) pool enriched with C18:0 fatty acyl chain generated by acyl-chain remodelling process. Furthermore, an extensive phylogenetic correlation analysis has revealed that Dip2 and PKC co-emerged and coevolved during early Opisthokonta evolution to establish the selective DAG-based PKC signalling axis.

**Results:**

**Dip2 is involved in the regulation of Pkc1-mediated cell wall integrity pathway**

Initial phenotypic screening revealed that Dip2 is necessary for the survival of yeast in various stress conditions like ER stress, osmotic stress etc (Mondal et al., 2022). However, *Dip2* knockout yeast (hereafter referred to as *Δdip2*) outperforms the wildtype (*WT*) strain under cell wall stress conditions (Mondal et al., 2022). This suggested a possible link between Dip2 and the cell wall integrity (CWI) pathway of yeast, which is governed by Pkc1 and the downstream mitogen-activated protein kinase (MAPK) signalling cascade. Given the requirement of DAGs for Pkc1 activation and the role of Dip2 in regulating DAG subspecies, we hypothesized that Dip2 maintains optimal levels of DAG subspecies necessary for activation of CWI pathway **(Fig. 1 A)**. To test this, we compared the fitness of *WT* and *Δdip2* yeast in the presence of cell wall stress-inducing agents like Congo red (CR) and Calcofluor white (CFW) (Roncero & Duran, 1985), using serial dilution assay in synthetic complete (SC) media (**Fig. 1 B**) as well as in rich media **(Fig. 1—fig. supplement 1)**. The two biological replicates, *Δdip2*_Colony1 and *Δdip2*_Colony2 showed increased resistance to cell wall stress, and the phenotype was restored through genetic complementation with Dip2 under its native promoter. Additionally, we

employed colony forming unit (CFU) assay for *WT* and *Δdip2* under cell wall stress. Counting the CFU also showed a similar and significant difference in the growth of *WT* and *Δdip2* colonies in the presence of CR **(Fig. 1 C)**. These observations suggest the regulatory role of Dip2 in CWI pathway of yeast. Since cell wall stress is associated with Pkc1-mediated activation of CWI pathway, we sought to test the status of Pkc1 signalling and its probable link to Dip2-regulated DAG subspecies. First, we probed the phosphorylation levels of a downstream MAPK effector of Pkc1 pathway, i.e., Slt2 (Suppressor of the LyTic phenotype) (Lee et al, 1993; Levin, 2005) to quantitatively assess the extent of Pkc1 activation. In agreement to the CWI phenotype, a ~3-fold increase in phosphorylation of Slt2 (pSlt2) was observed in *Δdip2* as compared to *WT*, where *WT* treated with CFW is used as a positive control for pSlt2 increase **(Fig. 1 D)**.

Next, we sought to understand if the hyperactivation of Pkc1 in *Δdip2* is DAG dependent and involves the catalytic activity of Dip2, i.e., conversion of selective DAGs to TAGs. To answer this, we generated two catalytic mutants of Dip2 ($Dip2^{D523A}$ and $Dip2^{L687A}$), that abolish its adenylation activity and have been shown to be unable to decrease the selective DAG levels on complementing *Δdip2*, as reported in our previous study (Mondal et al., 2022). The mutants were cloned under its native promoter in pYSS01 plasmid and expressed in *Δdip2* strain **(Fig. 1—fig. supplement 2A)**. The mutants could not diminish the cell wall stress resistance in *Δdip2*, unlike wildtype Dip2 **(Fig. 1 E)**. Additionally, complementation with the catalytically inactive Dip2 could not bring back the pSlt2 level in *Δdip2* **(Fig. 1—fig. supplement 2B)**, suggesting a direct correlation between the enzymatic activity of Dip2 and Pkc1 hyperactivation. Hence, the catalytic activity of Dip2 *i.e.*, the regulation of DAG subspecies level is essential in maintaining the active pool of Pkc1 for optimal CWI signalling.

Additionally, to confirm that the cell wall stress resistance observed in *Δdip2* is Pkc1 mediated, we inhibited Pkc1's activity using cercosporamide, a selective Pkc1 inhibitor

(Sussman et al, 2004) and observed decrease in the resistance to cell wall stress **(Fig. 1 F)**. The increase in pSlt2 level in *Δdip2* was also brought back to *WT* level upon treatment with cercosporamide **(Fig. 1 G)**. This implies that the hyperactivation of Pkc1 in *Δdip2* causes the cell wall stress resistance.

These observations intrigued us to ask how Dip2 spatially regulates Pkc1 as both reside at different subcellular locations inside the cell. Since Pkc1 is a bud site and plasma membrane localizing protein (Andrews P. and Stark M., 2000), we wondered whether Dip2 translocates to plasma membrane under cell wall stress. To examine this, we used *WT* strain with endogenous Dip2 tagged with GFP and subjected it to cell wall stress. As Dip2 predominantly localizes to the mitochondria, we co-stained cells with Mitotracker Red and found that there is no change in the spatial organization of Dip2 **(Fig. 1—fig. supplement 3)**. This suggests that Dip2 and Pkc1 could be cross talking through other ways that are yet to be explored.

**Dip2-regulated DAG subspecies activate Pkc1 signalling via selective interaction**

Since Dip2 is known to regulate the levels of C36:0 and C36:1 DAGs in yeast, we asked whether these specific DAG subspecies play any role in activation of Pkc1 signalling. Firstly, we examined how the system responds to cell wall stress in terms of the DAG levels. While tracking the Pkc1 signalling at temporal scale, we observed profound activation of Pkc1 pathway after 20-30 minutes of CFW treatment **(Fig. 2—fig. supplement 1A)**. Hence, we performed the lipidomic analysis of *WT* yeast pulse-treated with CFW for 30 minutes. Interestingly, the CFW treatment resulted in several fold increase in selective DAGs which normally constitute only 4-5% of the total DAG pool. We observed a ~8-fold increase in C36:0 DAGs and ~6-fold increase in C36:1 DAG subspecies levels compared to the untreated *WT* sample, while the other DAG species levels remained unaffected (**Fig. 2 A**). Thus, the data

clearly indicates that Pkc1 activation in yeast might require C36:0 and C36:1 DAG subspecies. We have also measured TAG subspecies levels in the presence of cell wall stress by CFW and observed that there is no depletion in the cognate TAG species suggesting that selective DAG accumulation upon CW stress is not due to TAG lipolysis **(Fig. 2—fig. supplement 1B)**.

Due to the seemingly high selectivity of DAGs for Pkc1 signalling activation *in vivo*, we sought to answer whether this specificity for C36:0 and C36:1 DAGs is engraved in the DAG binding domain of Pkc1. Therefore, to unravel the specificity of Pkc1 to interact with DAG across subspecies level, we performed an *in vitro* lipid binding assay. For this, we purified the DAG-binding domain of yeast Pkc1, namely conserved region domain 1 (C1domain), expressed under the galactose-inducible promoter in yeast, with GFP at its C-terminal **(Fig. 2—fig. supplement 2A).** Then, we performed liposome sedimentation assay where we prepared liposomes containing phosphatidylcholine (PC) with DAGs of different acyl chain compositions (DAGs were restricted to commercially available ones that are also abundantly present in yeast. C36:1 DAG is commercially unavailable). After incubating different liposomes with the protein, we separated both lipid-bound and unbound fractions and probed with western blot **(Fig 2 B)**. Surprisingly, we observed binding only in the fraction containing C36:0 liposomes, while there was no binding seen in any other DAG-containing liposome **(Fig. 2 C)**. Furthermore, we also observed a concentration-dependent increase in the binding of C1 domain with C36:0 DAGs **(Fig. 2 D and 2 F)**, confirming their direct physical interaction. On the other hand, no effect on binding was seen even at the higher concentrations of the other DAG species containing liposomes **(Fig. 2 E-F)**. This points to a clear specificity of the C1 domain of yeast Pkc1 for the selective DAG subspecies acted upon by Dip2. A negative control for GFP was also used to rule out any possibility of non-specific binding with GFP **(Fig. 2—fig. supplement 2B).**

We further asked whether a similar kind of selectivity of Pkc1 C1 domain for Dip2-regulated DAGs exists in higher eukaryotes as well. We cloned the C1 domain of one of the novel Pkc1s of *Drosophila melanogaster* (PKC98E) and rat (PKCδ), as yeast Pkc1 knockout phenotype has been shown to be rescued by mammalian novel PKCs (PKCδ) (Saiz-Baggetto et al., 2023), suggesting functional homology between the two. After expressing and purifying the C1 domains **(Fig. 2—fig. supplement 3A)**, we performed the liposome sedimentation assay and observed that PKC98E C1 domain binds the DAGs which were observed to be majorly accumulated in Δ*Dmdip*2 i.e., C32:0 and C34:1 DAGs (Mondal *et al*., 2022). Interestingly, C36:0, which was not changed significantly on deleting *DIP2* in *Drosophila*, is also found to bind the C1 domain of PKC 98E **(Fig. 2—fig. supplement 3B)**. This could possibly be due to the difference in the *in vivo* and the *in vitro* DAG specificity of Dip2 and Pkc, respectively. Since the lipidomic profile of the *Drosophila DIP2* deleted strain depicts the DAG changes from its whole-body tissue, it fails to provide an accurate picture of tissue-specific DAG specificity of Dip2, which would correspond to PKC.

Similarly, for rat PKCδ C1 domain, the liposome binding assay resulted in its binding with all the three DAGs tested (C32:0, C34:1, C36:0) **(Fig. 2—fig. supplement 3C)** which also corroborates our previous finding, where we observed the accumulation of multiple DAGs on knocking-out *DIP2A* from mouse embryonic cells (Mondal *et al*., 2022). Though this indicates a lack of DAG-specificity in Dip2 and PKC of higher eukaryotes, the presence of multiple paralogs of Dip2 and PKC isoforms complicate the identification of clear DAG selectivity. However, the correlation between the lipidomics data from Dip2A knockout mouse embryonic cells and the liposome sedimentation assay for PKCδ further strengthens our hypothesis that Dip2-regulated DAG species are involved in activation of PKCs across life forms.

## The canonical DAG metabolism axis is not involved in Pkc1 signalling

Since selective DAG-metabolism by Dip2 is associated with Pkc1 signalling, we asked whether manipulating the levels of bulk DAGs inside cell, mainly produced through canonical DAG metabolism can regulate Pkc1 signalling. DAG, being a central intermediary molecule in lipid metabolism, is acted upon by several conserved enzymes for phospholipid biosynthesis or storage lipid (TAGs) production. Majority of the enzymes participating in these processes are known to act on the bulk pool of DAGs, while the specificity for acyl-chain length remains to be elucidated (Li et al, 2020; Rockenfeller et al, 2018). Therefore, we probed two main TAG-forming enzymes, DAG acyltransferase (Dga1) and DAG transacylase (Lro1) along with the key membrane biogenesis enzyme, DAG kinase (Dgk1) for studying the effect of bulk DAG pool on Pkc1 activation and CWI pathway. Our lipidomic analysis of these gene knockouts confirmed that both Dga1 and Lro1 act on almost all the major DAG species and their absence led to ~2-10-fold accumulation of DAGs, consisting of varying chain lengths (**Fig. 3 A and 3 B**). *Δdgk1*, on the other hand, did not affect the steady-state DAG levels in yeast (**Fig. 3 C**), which is in agreement with earlier studies (Adeyo et al, 2011; Li et al., 2020). Surprisingly, none of the mutants of these bulk DAG-acting enzymes showed cell wall stress resistance in the presence of CFW (**Fig. 3 D**) or CR **(Fig. 3—fig. supplement 1)**. Quantifying the pSlt2 level in these knockouts also resulted in no change, when compared to total Slt2 levels **(Fig. 3 E)**.

To understand how Dip2 responds to the accumulation of bulk DAGs inside the cells, we probed the localization of Dip2 in the absence of *LRO1* and *DGA1*. Upon co-staining the cells with Mitotracker Red, we found that Dip2 remains in the mitochondria **(Fig. 3—fig. supplement 2)**. This suggests that the bulk DAG accumulation does not affect Dip2 subcellular localization. This might also be due to the spatial segregation of the bulk DAG pool in the endoplasmic reticulum from the selective DAG pool, which is likely to be present in mitochondria or mitochondria-vacuole contact sites.

In addition, we also generated double deletion mutant of *DGA1* and *LRO1* and quantified the DAG levels **(Fig. 3 F)**. Spot assay for the double knockout shows that they are sensitive to cell wall stress in the presence of CFW **(Fig. 3 G)** and in the presence of CR **(Fig. 3—fig. supplement 2B)**. However, there was ~1.6-fold increase in pSlt2 level compared to *WT*, which is half of what we observe in *Δdip2* (3-fold) (**Fig. 3 H**). Thus, despite having a ~2 to ~3.5-fold accumulation of total DAG pool in the absence of canonical enzymes, Pkc1 mediated CWI signalling remained unaffected. These observations establish that there is a functional dichotomy in the cellular DAG pools: a metabolically active DAG pool that only participates in lipid biogenesis activities and signalling DAG pool that activates Pkc1 signalling cascade. Therefore, it can be proposed that the Dip2-mediated selective DAG axis has been evolved to utilize a DAG subpopulation as a secondary messenger to facilitate the regulation of PKC activation.

**Dip2-regulated DAG subspecies for Pkc1 activation originate from phosphatidylinositol and its acyl-chain remodelling by Psi1**

Since canonical DAG metabolism pathway is decoupled from Pkc1 signalling, we sought to identify the source of Dip2-regulated DAG subspecies involved in Pkc1 activation. We probed major metabolic routes that can possibly contribute to specific DAG accumulation in *Δdip2*. We treated *WT* and *Δdip2* with various inhibitors with the aim to cut off the supply of DAGs from respective lipids (shown as schematic in **(Fig. 4 A)**) and checked for the reduction in DAG accumulation. Interestingly, inhibition of PI(4,5)$P_2$ (hereafter referred to as PIP2) to DAG conversion by U73122, a Phospholipase C (PLC) inhibitor (Banfic et al, 2013; Jun et al, 2004), reduced the specific DAG levels by 80-90% in a concentration-dependent manner **(Fig. 4 B)**, while the other DAG species remained unaffected **(Fig. 4—fig. supplement**

**1A)**. On the other hand, blocking PA to DAG as well as ceramide to DAG synthesis using propranolol and aureobasidin-A, respectively (Breslow et al, 2010; Morlock et al, 1991; Sasser et al, 2012; Starr et al, 2016), did not show change in DAG levels **(Fig. 4—fig. supplement 1B-C)**. To confirm the same, we also generated double knockout of *DIP2* and the major PA to DAG producing enzyme genes in the cell, i.e., *PAH1* and checked for DAG accumulation. We found that unlike what we observed in propranolol-treated *Δdip2* which showed no change in DAG level, double knockout of *PAH1* and *DIP2* showed ~1.5-to-2-fold increase in all the bulk DAGs (C32:1, C32:2, C34:1) **(Fig. 4—fig. supplement 2A)**. However, we also observed a significant decrease of ~42% in C36:0 and ~81% in C36:1 DAGs. We also probed the effect of *PAH1* deletion on CW stress pathway and Pkc1 activation. We found that *Δpah1* and *Δpah1Δdip2*, both are defective in growth and sensitive to CW stress **(Fig. 4—fig. supplement 2B)**. This phenotype does not correlate with pSlt2 level **(Fig. 4—fig. supplement 2C)**, suggesting that the CW stress sensitivity is not linked to Pkc1 activation and may indicate a pleotropic defect due to alteration in lipid metabolism. However, given the reduction in the level of selective DAGs in *Δpah1Δdip2*, we cannot rule out the possibility that Pah1 could also be contributing to the selective DAG accumulation in *Δdip2*. Given this observation, we also asked whether the absence of Pah1 could affect subcellular localisation of Dip2. Therefore, we used microscopy to trace Dip2 in *Δpah1* and found no change in its localization suggesting that Pah1 deletion has no impact on Dip2 localization **(Fig. 4—fig. supplement 2D-E)**.

We also deleted *PLC1 in Δdip2* and observed a ~75% reduction in C36:0, C36:1 DAGs **(Fig. 4 C)**, with no change in other DAG species**,** suggesting that Plc1-dependent hydrolysis of C36:0 and C36:1 PIP2 pools serves as the predominant source of Dip2-metabolised selective DAGs. Whether the same source of DAGs is responsible for Pkc1 activation was investigated by checking *pSlt2* levels. *Δplc1Δdip2* and U73122-treated *Δdip2* showed depleted levels of *pSlt2*, when compared to *Δdip2*, while Slt2 phosphorylation remained unaffected in *Δplc1* **(Fig.**

**4 D)**. This suggested that the DAGs regulated by Dip2 are sourced via hydrolysis of corresponding PIP2 and are further involved in activating Pkc1 pathway. However, a further depletion of pSlt2 level in *Δplc1Δdip2*, compared to *Δplc1* was surprising as deletion of *DIP2* should not alter the level of pSlt2 level. This might have resulted from a rewiring of pathways upon deleting both the genes, which possibly led to a pleiotropic effect. These observations were also strengthened by the live-cell imaging of Plc1 that showed that Plc1 partially localizes to the mitochondria **(Fig. 4—fig. supplement 3A-B)** and vacuoles **(Fig. 4—fig. supplement 3C-D)**, similar to Dip2 suggesting that it might be producing the selective DAGs locally for Dip2 to act upon.

Next, we asked how exactly the specific PIP2 pool is maintained inside the cell to source these DAGs. Strikingly, a previous study has reported that the absence of an acyltransferase, phosphatidylinositol stearoyl incorporating 1 (Psi1), leads to severe depletion of C36:0 and C36:1 PIP2 species. Psi1 remodels the neo-synthesized phosphatidylinositol by adding stearic acid (C18:0) at the *sn-1* position of its glycerol backbone (Le Guedard et al, 2009), thus enriching the PI and eventually PIP2 pool with specific acyl chains (Doignon et al, 2016). Hence, we checked the DAG levels in *Δdip2* upon deleting *PSI1* (*Δpsi1Δdip2*) and observed a significant decrease in the accumulated DAGs (**Fig. 4E**). It is worth noting here that *PSI1* deletion in *Δdip2* background did not lead to complete depletion of accumulated DAGs in *Δdip2*, but a considerable quantity of DAGs, i.e., ~36% of C36:0 and 40% of C36:1, respectively are channelled from Psi1. In the single deletion of *PSI1*, unexpectedly, we observed increase in almost all the DAGs quantified **(Fig. 4—fig. supplement 4)**, which could be because of a compensation effect the system might have adapted due to decrease in C36:0, C36:1 phosphoinositide and respective DAGs, as reported earlier (Doignon et al., 2016). To test its role in Pkc1 activation, we measured pSlt2 levels in *Δpsi1Δdip2* and found that pSlt2 levels restored back to *WT* levels **(Fig. 4 F)**. In fact, deletion of *PSI1* itself decreases the pSlt2 level

in *WT* by ~35%, which phenocopies *Δpsi1Δdip2,* thereby strengthening the contribution of Psi1 to Pkc1 activation.

Together, these observations emphasize that the acyl chain remodelling of PI by Psi1 for specifically enriching C36:0 and C36:1 ensures channelling of these chain length compositions towards respective PIP2. The corresponding PIP2 species are then hydrolysed to selective DAGs by Plc1, which is responsible for Pkc1 activation. Dip2, which acts on these DAGs, regulates Pkc1 signalling and keeps a check by converting these DAGs to TAGs (**Fig. 4 G**). In addition, these observations also reiterate that the bulk DAG pool cannot activate Pkc1 signalling cascade. Therefore, the Psi1-Plc1-Dip2 axis serves not only as a source of DAGs but also acts as a critical checkpoint for the Pkc1 signalling cascade.

**Co-emergence and coevolution of Dip2-PKC axis underscores the selective nature of DAG-based signalling**

DAGs are universally recognised by a structurally conserved domain called C1 domain (conserved domain 1) (Hurley et al, 1997), found in different DAG effector proteins including PKC. To understand the evolutionary relationship between DAG effectors and selective DAG regulator, Dip2, we probed their distribution across the tree of life. Previously, we showed that Dip2 had emerged in early opisthokonts. Interestingly, phylogenetic distribution of all known DAG effectors (Colon-Gonzalez & Kazanietz, 2006) revealed that the majority of these are concentrated in metazoans and metazoan sister groups (Choanoflagellates, Filasterea and Ichthyosporea), while PKC is the only DAG effector conserved in fungal groups and all opisthokonts **(Fig. 5 A)**.

Fungal Pkc1 (hereafter referred to as prototypical PKC) (Schmitz & Heinisch, 2003) harbours all the typical regulatory domains present in higher eukaryotes, which includes HR1 (homology region 1) domain, C2 domain (conserved domain 2), C1 domain (conserved domain 1) along with the protein kinase domain (Schmitz & Heinisch, 2003). The phylogenetic distribution suggest that the prototypical PKC had probably undergone multiple gene duplication, domain shuffling and gene loss events during early metazoan evolution resulting in a repertoire of PKC isoforms **(Fig. 5—fig. supplement 1A)**. Furthermore, we observed the presence of primitive PKC, consisting of only C1 and protein kinase domains in Microsporidia, the sister group of Fungi (Bass et al, 2018; James et al, 2013). Interestingly, only two *Dictyostelium* species of protists out of ~50 genomes (available in KEGG database) harbour PKC in its primitive form (Goldberg et al, 2006; Keenan et al, 1997; Wang et al, 1996). Thus, the early DAG effectors with C1 domain had evolved in one of the two major eukaryotic branches, known as Unikonta (comprising protist, microsporidia, fungi and metazoa). To our surprise, the other eukaryotic branch, Bikonta, comprising of plants, algae and SAR **(S**tramenopiles, **A**lveolates, and **R**hizaria) organisms, is completely devoid of the DAG effectors (**Fig. 5 A**). Overall, our analysis suggests that PKC is the first DAG effector to be recruited in eukaryotes and evolved exclusively in opisthokonts.

The emergence of a prototypical Pkc with DAG-binding C1 domain in early opisthokonts suggests potential requirement of DAG regulators for optimal signalling process. Previously, we have reported that FAAL-like domains from bacteria gave rise to two tandem FAAL-like domain containing protein, Dip2 across fungi and metazoans (Mondal et al., 2022; Patil et al, 2021). Interestingly, the phylogenetic profile analysis of PKC **(Fig. 5—fig. supplement 1B)** and Dip2 showed that both are distributed across Fungi and Animalia, but are totally absent from Archaea, Bacteria, Plantae and Algae, suggesting that both the proteins show evolutionary co-emergence and co-occurrence (**Fig. 5 B**). It is important to note here that

Dip2 is absent in a major phylum of fungi called Basidiomycota, suggesting a possible gene-loss event in this phylogenetic branch. Although Basidiomycota harbours C1 domain containing Pkc1, whether the Pkc1 is regulated by an unknown functional orthologue of Dip2, or a distinct Pkc1 signalling has been evolved in this branch of fungi, is yet to be understood. Taken together, our analysis underscores the fact that the emergence of a fully functional PKC signalling pathway can be marked by the presence of Dip2 from fungi onwards.

To investigate the evolutionary history of Psi1-Plc1 axis, we examined the phylogenetic distribution pattern and found that Psi1 was evolved in early eukaryotes and is conserved in both Unikonta and Bikonta. On the other hand, Plc1, consisting of multiple domains such as PH domain, EF hand domain, PI-PLC domain and C2 domain, emerged in protists and is distributed across Unikonta, while absent in Bikonta **(Fig. 5—fig. supplement 1C)**. This evolutionary history parallels that of the relevant DAG effector, PKC.

We then sought to quantitatively assess the phenomenon of co-evolution between Dip2 and PKC. To investigate this, we furthered our bioinformatic analysis using molecular phylogenies of Dip2 and PKC from the representative fungi across fungal divisions (Ocana-Pallares et al, 2022). Correlation between the phylogenetic distances (patristic distance) of Dip2 and PKC were calculated using multiple methods like Bayesian method, neighbour joining, minimum-evolution, and maximum likelihood (Fourment & Gibbs, 2006). The result showed significantly high association in the pairwise patristic distances of Dip2 and PKC, compared to other control gene pairs like Pgk1 and Gapdh **(Fig. 5 C-D)**, suggesting their possible co-evolution across fungal phylogenetic branches.

To calculate the interspecies correlation of genetic divergence rate, we adopted the approach described for mirrortree algorithm (Edgar et al, 2012; Ochoa & Pazos, 2014; Pazos & Valencia, 2001). In this case, genetic distances (distance matrix-based) were used to estimate

the evolutionary association between Dip2 and PKC (**Fig. 5E)**, which scored more than a correlation coefficient of 0.8, an empirical cut-off value suggested by (Pazos & Valencia, 2001). We further reconfirmed the above observation using a larger set of all available fungal genomes **(Fig. 5—fig. supplement 2A)**. This observation is further substantiated by a lesser correlation obtained on comparing Dip2 or PKC with a highly conserved gene like *GAPDH* **(Fig. 5E)**. Furthermore, the correlation between *DIP2* or *GAPDH* and a diverse set of conserved genes with related and unrelated functions were found to be below the cut-off value of correlation coefficient (<0.8) (**Fig. 5F and fig. supplement 2B)**. We also confirmed that the correlation between Dip2-PKC pair is significantly different from this random control set **(Fig. 5—fig. supplement 2C-D)**. Therefore, a significant interspecies correlation between Dip2 and PKC suggested that both the genes had experienced a similar evolutionary pressure, probably due to their participation in the same physiological axis. Overall, the evolutionary analysis suggests that Dip2 and PKC are phylogenetically correlated and have coevolved together for successful establishment of selective DAG-based PKC signalling in Opisthokonta.

**Discussion:**

The discovery of Dip2 as a conserved and selective DAG regulator presented a cellular scenario, where there are two 'functional' pools of DAG in cell, *viz*., the bulk 'metabolic' pools of DAG and the minor pools of 'signalling' DAG. The former is involved in membrane biogenesis and storage lipid biosynthesis, while the later is Dip2-regulated selective DAG pool, responsible for activating Pkc1 signalling. Here, we provide evidence for the emergence of Dip2 and the functional diversification of DAG pool, responsible for activation of Pkc1 signalling cascades in yeast. As DAG metabolizing enzymes are generally promiscuous, their recruitment for selectively activating and fine-tuning the Pkc1 signalling events is a distant

possibility. The rooting of a lipid-based signalling in eukaryotes during early Opisthokonta evolution possibly necessitated a more precise regulatory mechanism, making a species-specific regulator such as Dip2 inevitable for DAG-based PKC signalling **(Fig. 6)**.

The metazoan PKC isoforms such as conventional and novel PKCs are well characterized to be regulated by signalling molecules such as DAGs, calcium, phosphatidylserine etc. (Rosse et al, 2010). Different combinations of regulatory domains in PKC isoforms result in highly diversified and mutually exclusive functions in animals (Reyland, 2009). Interestingly, the single prototypical PKC of yeast with all the regulatory domains is involved in a myriad of physiological processes, for example, cell wall organization, progression of cell cycle, lipid metabolism, cell polarity, p-body assembly, septin organization etc. (Dey et al, 2017). Initially, Pkc1 activation was shown to be unaffected by DAGs (Antonsson et al, 1994), while a few recent reports have suggested the involvement of DAGs in activating Pkc1 *in vitro* (Dey et al., 2017). We believe the discrepancy among the existing reports has been cleared as we have observed a selective DAG-mediated Pkc1 and CWI pathway activation in yeast. The earlier observed mutations in the putative DAG-binding C1 domain of yeast Pkc1 which results in decreased fitness in cell wall stress conditions (Jacoby et al, 1997), corroborates our findings on the crucial role of DAG in activation of Pkc1-based CWI pathway. Similarly, a differential role of other domains like HR1 has been proposed in earlier studies (Schmitz et al, 2002). Whether the selective DAG-based Pkc1 activation also requires HR1 domain to bind Rho1, remains to be seen.

Recent reports have shown that exogenous addition of DAGs with varied acyl chains have differential effect on the translocation of mammalian PKC isoforms (Schuhmacher et al., 2020). While this indicates the role of distinct acyl chain-containing DAGs in differentially activating PKC isoforms, it does not represent a physiological scenario where a cell employs this. Here, we have shown selective increase in C36:0 and C36:1 DAGs which results in

activation of Pkc1 upon subjecting the yeast cells to cell wall stress. Additionally, the DAG binding domain of Pkc1 shows binding exclusively with C36:0 DAG and not with other DAGs *in vitro*. Hence, we have identified the specific DAG subspecies for regulating Pkc1, thereby, bridging the gap in the understanding of selective DAG-driven PKC activation, that was speculated thirty years ago (Marignani et al., 1996). Nonetheless, the rationale for selecting the two DAG subspecies out of numerous possible combinations of acyl chains for activating Pkc1 remains an enigma and needs to be probed. It also opens up possibilities for specific roles of selective species of lipids that perhaps explains why there is a preservation of diversity in lipidome during evolution of different life forms.

The canonical DAG metabolizing enzymes, despite acting on C36:0, C36:1 DAGs to a certain level, are excluded from their regulatory role in Pkc1 signalling. Although the double deletion of *LRO1* and *DGA1* elevates Pkc1 activation to an extent, this increase is insufficient to confer resistance to cell wall stress. Whether it is the distinct source of Dip2 regulated DAGs from the PI pool or the spatial segregation of the two pools inside the cell, which make it exclusive to Pkc1 pathway regulation needs to be probed. Furthermore, how Pkc1, which is a bud-site (plasma membrane) protein in yeast (Denis & Cyert, 2005), is regulated by a selective DAG regulator Dip2 residing at mitochondria-vacuole contact site (Mondal et al., 2022) requires further investigation. Characterizing the spatiotemporal nature of specific DAG accumulation that drives these processes would provide clues to the partitioning of Pkc1 activity and is currently underway.

Although, PKC is a well-studied signalling proteins and DAG-PKC signalling has been a textbook model for several decades, the evolutionary and regulatory origin of this pathway remained unknown. Our current work provides compelling evidence that suggests that PKC was the first DAG effector protein to be evolved and conserved in opisthokonts, while completely absent in the other eukaryotic supergroup Bikonta which comprises plant, algae

and SAR organisms. The evolution of such distinct lipid-based signalling in early eukaryotic ancestors is probably a decisive factor for further branching into two subgroups- Unikonta (mainly Opisthokonta) and Bikonta. Thus, the work also suggests that the emergence of Dip2 around 1.2 billion years ago in Opisthokonta was a unique metabolic innovation to establish a precisely regulated PKC signalling pathway (**Fig. 6**).

The role of Dip2 in fungal virulence has been highlighted in several studies as its deletion in various plant and animal pathogenic fungi like *Magnaporthe oryzae* (causing rice blast), *Cochliobolus heterostrophus* (causing southern corn blight) and *Coccidioides posadasii* (causing valley fever) renders them avirulent (Lu et al, 2003; Narra et al, 2016; Wang et al, 2016). As PKC signalling has also been shown to be crucial for pathogenicity of fungi, the identification of Dip2 as a unique regulator of PKC would open avenues for therapeutic and pharmacological interventions. Similarly, the phenotypes for PKC hyperactivation and deletion of Dip2 observed independently in animals suggest a link between Dip2 and regulation of PKC isoforms. For instance, the abnormalities observed in upregulation of different PKC isoforms such as axonal bifurcation and outgrowth (Nitta et al, 2017; Zhang et al, 2019), altered dendritic spine morphogenesis (Calabrese & Halpain, 2005; Ma et al, 2019) etc. phenocopy the defects reported in Dip2 knockouts (Ma et al., 2019; Nitta et al., 2017). Moreover, both Dip2A and PKC have been implicated independently in autistic behaviour in model organisms (Liu et al, 2018; Ma et al., 2019; Philippi et al, 2005). Similarly, loss of Dip2C, a candidate breast cancer gene (Li et al, 2017), leading to increased epithelial-mesenchymal transition (EMT) in cancer cell lines (Larsson et al, 2017), also resembles PKCε overexpression, which not only induces EMT but is also a biomarker for aggressive breast cancer (Jain & Basu, 2014). These observations provide a rationale to test the possibility that multiple paralogs of Dip2 might be regulating various PKC isoforms by acting on specific pool of DAGs in higher eukaryotes.

## Materials and methods:

### Yeast strains and plasmids

Yeast strains used in this study are all BY4741 (MATa ura3Δ0 his3Δ1 leu2Δ0 met15Δ0) (Brachmann et al, 1998) derived from S288C genetic background as listed in (**Appendix 1 table 1**). Single gene knockout strains are retrieved from the public repository Euroscarf, except for *Δdip2* which is generated by homologous recombination from our previous study (Mondal et al., 2022).

Galactose promoter was replaced by the native Dip2 promoter in the plasmid pYSM10 used in our previous study using Gibson assembly cloning. This was also used as the template for site-directed mutagenesis by performing polymerase chain reaction using mutagenic oligonucleotides. These mutants were confirmed by sequencing.

Double knockout strains of *Δpsi1Δdip2* and *Δplc1Δdip2* were generated by knocking out *DIP2* from *Δpsi1* and *Δplc1* strains from Euroscarf library by homologous recombination. Briefly, *Dip2* (Cmr2; SGD ID: S000005619) gene was replaced with a PCR amplified hygromycin resistance cassette from pFA6A-hphMX6 plasmid. The primers were designed in such a way that the PCR product will have flanking sequences homologous to the 5′ and 3′ end of *DIP2* gene. The PCR product was purified and transformed using direct carrier DNA/PEG method-based transformations (Gietz & Schiestl, 2007). Transformed cells were plated on both hygromycin and G418 selection plate for *DIP2* and *PSI1/PLC1* deletion respectively. Thus, the resistant colonies were further validated for deletion using PCR primers amplifying the hygromycin cassette, designed using a web tool Primers-4-Yeast (Yofe & Schuldiner, 2014) as listed in (**Appendix 1 table 2**). Dip2 was tagged with GFP in the knockout strains of *LRO1* and *PAH1* by transforming amplicons produced by using Dip2 specific C-tag primers, using pFA6A-HisMX6 plasmid. For generating Dip2-GFP in *Δdga1*, we transformed Dip2 tagged with GFP under its native promoter in the double knockout of *DIP2* and *DGA1*. All the GFP

tagging was confirmed by western blot using anti-GFP antibody. For C1a-C1b protein expression, C1a-C1b (413-534 aa) was amplified from yeast genomic DNA and cloned into galactose inducible pYSM5 vector used in our previous study (Mondal et al., 2022).

**Media and reagents**

Yeast cells were grown in synthetic complete (SC) media, at 30°C in a shaking incubator with 200 rotation per minute (RPM). SC media constituents include 1.7 g/l yeast-nitrogen base with ammonium sulphate (BD Difco), 20 g/l glucose supplemented with appropriate amino acids (Sigma), adenine (Sigma A5665) and uracil (Sigma U0750). G418 (200 µg/mL) and Hygromycin (0.2mg/mL) were used for knockout strain selection. For some experiments, YP media (yeast extract – 10 g/l, peptone – 20 g/l) supplemented with 2% dextrose was used. 2% bacto agar along with the above-mentioned SC media constituents was used for solid media.

**Spot assay**

An overnight primary culture in SC media was diluted to 0.5 $OD_{600}$ nm and grown till the secondary culture reaches $OD_{600}$ nm of ~2.0. This culture was diluted to 0.2 $OD_{600}$ nm and was used as the first dilution, which was further diluted into multiple serial dilution stocks ($10^{-1}$, $10^{-2}$, $10^{-3}$, and $10^{-4}$). 10 µl of each dilution stocks were spotted sequentially on SC agar control plate and SC agar with either Congo red (100 µg/mL) (Sigma) or Calcofluor white (Sigma) (50 µg/mL) to induce cell wall stress or in combination with cercosporamide (2 µg/mL).

**Colony forming unit assay**

A primary culture was inoculated overnight and was diluted to 0.2 $OD_{600}$ nm in fresh SC media, cultured till the early log phase or $OD_{600}$ nm of ~0.8. Cells were serially diluted to 0.002 $OD_{600}$ nm in autoclaved filtered Milli-Q water and 80µL of the cells were plated on SC media agar as well as SC media agar with CR. After incubation for ~48 hours at 30°C, number of colonies were counted and CFU was calculated.

**Growth curve analysis**

The overnight grown primary culture of *WT* and *Δdip2* was inoculated in fresh SC media with ~0.2 $OD_{600}$ nm. Growth curve was performed using this secondary culture grown with and without CR. The cell density was measured starting from an $OD_{600}$ nm of 0.2 at zero time point to 28 hours. The readings were recorded at an interval of every 4 hours, until it reaches the stationary phase.

**Protein expression and purification**

C1-GFP (413-534 amino acids) tagged with GFP and 8xHis at its C-terminus was expressed in *S. cerevisiae*. Wherein, 8L cell culture grown in YP-Galactose media for induction was harvested at 4000 RPM and was resuspended in buffer A (PBS pH 8.0, 500 mM NaCl, 10% Glycerol and 5 mM β-mercaptoethanol), protease inhibitor cocktail (PIC), 1mM phenylmethysulfonyl fluoride (PMSF) and lysed using 0.5 mm glass beads. For the expression check, cell lysate was mixed with 6X-SDS loading dye and was run on 12% SDS gel and checked for in-gel GFP fluorescence. The protein was purified by affinity chromatography with nickel-nitrilotriacetic acid (Ni-NTA) agarose beads using buffer A. Protein was eluted by single-step elution using Buffer A containing 250 mM imidazole. Following elution, the protein was buffer exchanged in Buffer B (PBS, 150 mM NaCl, 10% Glycerol, 2mM DTT), concentrated and stored at -80°C until further use.

The C198E (a.a. 171-304 of *Drosophila* PKC98E) and C1 delta (a.a. 152-280 of mouse PKC delta) genes were cloned into pETite vector (Lucigen, USA) with a C-terminal TEV cleavage site, GFP and 6x His tag. E. coli HI-control BL21(DE3) (Lucigen, USA) cells were used for expression using Isopropyl β- d-1-thiogalactopyranoside (IPTG) induction-based overexpression. Cells were grown at 37°C until the O.D. reached 0.6-0.8 and then induced using 0.5mM IPTG and incubated at 18°C for 16 hours. After induction, the cells were harvested at 7000rpm for 5 minutes at 4°C. Purification was done according to previously published protocols (ref.). Briefly, the proteins were purified by immobilised Ni-NTA based affinity chromatography in buffer containing 50mM Tris-HCl pH 8.0, 300mM NaCl, 0.4% Triton X-100 and 1mM PMSF. The proteins were eluted using gradient elution between 10 and 250mM imidazole. Eluted proteins were further purified by size-exclusion chromatography using Superdex 200 in buffer containing 20mM Tris-HCl pH 8.0, 150mM KCl. Fractions were pooled, concentrated and stored at -80°C until further use.

**Liposome co-sedimentation assay**

Liposomes were prepared according to previously published (Dey et al., 2017; Larsson et al, 2020). Briefly, Lipids (800 nano moles of POPC (Avanti polar lipids) and 200 nano moles of DAGs (Sigma) for 20 mole percent, were dissolved in chloroform: methanol (2:1 v/v), mixed in glass tubes and dried to thin film under nitrogen gas stream. Following overnight desiccation, 1mL of Hydration buffer (50mM Tris-HCl pH 7.5, 150mM NaCl, 10mM $MgCl_2$, 1.7mM $CaCl_2$, 10mM β-mercaptoethanol) was added to make 1mM final lipid concentration. The tubes were vortexed vigorously and subjected to 10 freeze-thaw cycles using liquid nitrogen for 1min and at 50°C water bath for 3 min.

C1-GFP (7nM) was incubated with liposomes for 10 minutes in ~~a total volume of~~ 300µl of hydration buffer. After incubation, the reaction mixture was centrifuged at 100,000xg for 1 hour at 4°C. The supernatant was collected in a separate tube and both supernatant and pellet were subjected to SDS-PAGE, followed by western blotting using Anti-GFP antibody (Cell Signalling Technology). An in-house linker of 11 amino acids attached with 8xHis and GFP at the C-terminal (DSLEFIASKLA-GFP) was purified and used to probe for GFP as a negative control. Images were captured in BioRad ChemiDoc imaging system and analysed using ImageJ.

**Western blotting**

Overnight grown yeast cells were inoculated in fresh YPD media (10 mL) at 0.2 $OD_{600}$ nm and grown till log phase (2-2.5 $OD_{600}$ nm). Cell pellets were harvested, washed with Phosphate buffered saline (PBS) and flash frozen using liquid-nitrogen. The pellets were then dissolved in 120 µl of Lysis Buffer (50 mM Tris-HCl [pH 7.5], 150 mM NaCl, 5 mM EDTA, 1% Nonidet P-40/Triton X-100, 1 mM Sodium Pyrophosphate, 1 mM Sodium Orthovanadate, 20 mM NaF, 1 mM Phenylmethylsulfonyl Fluoride, 1% Protease Inhibitor Cocktail (Nomura & Inoue, 2015). The dissolved pellets were subjected to lysis with glass beads on a mechanical vortex for 10 cycles of 30 s. The obtained homogenate was centrifuged at 12000 rpm for 10 min at 4˚C and then the supernatant was boiled with LaemmLi buffer for 15 min. Protein extracts were separated on SDS-PAGE and then transferred on to PVDF membrane (Millipore) using wet transfer at 100 V for 2 hours. Membranes were blocked using 5% BSA in Tris-buffered saline with 0.1% Tween 20 detergent (TBST) and then incubated with appropriate primary antibodies (Anti-Phospho-p44/42 MAPK (Erk1/2) (Thr202/Tyr204) Cell Signalling Technology #9101) to measure pSlt2 and p44/42 MAPK (Erk1/2) Antibody Cell Signalling Technology #9102) (Sariki et al., 2019) to measure total Slt2 at 1:5000 dilution or TPI1 at

1:10000 dilution (gift from Dr. Palani Murgan's lab, CSIR-CCMB) followed by washing and incubation with secondary antibody (Anti-rabbit IgG Cell Signalling Technologies #7074 (1:10000). After final wash with TBST, bands were visualised using SuperSignal™ West Pico PLUS chemiluminescent horseradish peroxidase (HRP) substrate using BioRad Imaging System. Images were analysed using ImageJ software. For cell wall stress, cells were incubated with CR or CFW for 30 min before harvesting. For cercosporamide treatment, cells were incubated for 30 min at a concentration of 5µg/mL followed by harvesting and sample preparation.

**Lipidomics sample preparation**

Yeast cells were grown overnight in SC media and were diluted in 20 mL media (x6 replicates, total 120 mL media for single strain) to 0.2 $OD_{600}$ nm, cultured and harvested at ~2-2.5 $OD_{600}$ nm. Inhibitor treated samples were cultured the same way, except that U73122 (0.5mM and 1mM) (Sigma), propranolol (1mM) (Sigma), aureobasidin A (0.025 µg/mL) (Takara) were added while inoculating for the secondary culture at 0.2 OD. For cell wall stress, cells were subjected to CFW (50µg/mL), 30 min before harvesting. Lipid isolation was performed following modified-Folch method as reported previously (Abhyankar et al, 2018; Kelkar et al, 2019; Kumar et al, 2019; Mondal et al., 2022; Pathak et al, 2018). Briefly, Cell pellets were washed with PBS and flash frozen in liquid nitrogen. Cells were resuspended in 500 µl of chilled PBS and were lysed using sonicator at 60% amplitude for 1 sec ON/ 3 sec OFF for 10 cycles with a probe sonicator on ice bed. 10 µl of lysate from each sample was collected for protein estimation required for data normalization during lipid analysis. 250 µl of PBS was added, followed by addition of $CHCl_3$ and methanol mix with respective internal standards to achieve the ratio of 2:1:1 ($CHCl_3$: Methanol: PBS). Mixture was vortexed thoroughly (2 cycles of 30 s) and was phase separated by centrifugation at 3000 RPM at RT. Bottom phase was

collected in fresh glass vials followed by addition of 100 µl of formic acid (~10%, vol/vol of lysate volume) to the remaining top phase. After vortexing again, the same way, same volume of $CHCl_3$, as mentioned in previous step, was added for re-extraction by phase separation. Bottom phase was pooled with the already separated lipid in the first round. The total lipids extracted were dried under stream of nitrogen at room temperature. Protein estimation was performed using Bradford assay reagent (Sigma).

## Lipidome analysis by mass spectrometry

The lipidomic experiment and analysis of the isolated lipid species were performed according to previously described protocols (Abhyankar et al., 2018; Kelkar et al., 2019; Kumar et al., 2019; Mondal et al., 2022; Pathak et al., 2018). Semi-quantitative analysis of lipids was performed using two mass spectrometers: An Agilent 6545 LC-QTOF (quadrupole-time-of-flight) and a Sciex X500R QTOF employing high-resolution auto MS-MS methods and multiple reaction monitoring high resolution (MRM-HR) scanning respectively. An Electrospray ionization (ESI) source was used in both mass spectrometers. The dried lipid extracts were re-solubilized in 200 µL of 2:1 CHCl3: MeOH and 10 µL was injected into the mass spectrometers.

The liquid chromatography separation protocol was the same for both instruments. A Luna C5 column (Phenomenex, 5 µm, 50 × 4.6 mm) coupled to a C5 guard column (Phenomenex, 4 × 3 mm) was used for LC separation. The solvents used were buffer A: 95:5 H2O: MeOH + 0.1% Formic acid + 10mM ammonium formate and buffer B: 60:35:5 iPrOH: MeOH: H2O + 0.1% Formic acid + 10mM ammonium formate. Methods were 30 minutes long, starting with 0.3 mL/min 100% buffer A for 4 minutes, 0.5 mL/min linear gradient to 100% buffer B over 14 minutes, 0.5 mL/min 100% buffer B for 7 minutes, and equilibration with 0.5 mL/min 100% buffer A for 5 minutes.

The following settings were used for the ESI-MS positive mode analysis on the Agilent 6545 LC-QTOF: drying gas and sheath gas temperature: 320 °C, drying gas and sheath gas flow rate: 10L/min, fragmentor voltage: 150V, capillary voltage: 4000V, nebulizer (ion source gas) pressure: 45 psi and nozzle voltage: 1000V. For analysis, a lipid library of DAGs and TAGs was employed in the form of a Personal Compound Database Library (PCDL), and the peaks were validated based on relative retention times and fragments obtained.

For the Sciex X500R QTOF, the following settings were used for the ESI-MS positive mode analysis: source gas temperature: 400°C, spray voltage: 4500V, source gas 1 pressure: 40 psi, source gas 2 pressure: 50 psi. Peaks were quantified using Sciex OS, where the masses of DAGs and TAGs were curated from the lipid maps structural database (LMSD).

All lipid species were quantified by normalizing areas under the curve to the protein concentration of the lysate taken at the beginning.

**Live Cell Microscopy**

Endogenous GFP-tagged strains were grown in SC media at 30°C and were harvested between 1.5-2 $OD_{600}$ nm (log phase). MitoTracker Red CMXRos (Invitrogen Inc) was added to a final concentration of 50 nM in 1 mL of liquid cell culture and was incubated further for 30 min with shaking. Cells were then washed 5 times with PBS and was resuspended in 20µl of PBS. 3µl of these cells were immobilized under agar bed on glass slides and visualized under a Zeiss Apotome.2, inverted widefield fluorescence microscope equipped with a HAL 100 illuminator, Plan Apochromat ×100 oil objective (NA 1.4), and a AxioCam CCD camera. Images were captured in DIC (Nomarski optics), mCherry (for MitoTracker Red) and FITC fluorescence mode. All images were processed using ImageJ2 software.

**Phylogenetic profiling**

Sequences for phylogenetic profiling were collected from a stringent BLAST hit search (Altschul et al, 1990) using the protein sequence from *Saccharomyces cerevisiae* as the query. A defined list of organisms was made in order to account for the diversity in the fungal kingdom (Ascomycota, Mucoromycota, Zoopagomycota, Blastocladiomycota, Chytridiomycota, Holomycota) for all the proteins used for coevolution analysis. For the distribution of PKC across tree of life, sequences were collected from the representative organisms from protists to metazoans, consisting of novel, conventional and atypical PKCs. The domain organization of the collected sequences was verified in Conserved Domains Database (CDD) (Lu et al, 2020) to filter partial sequences. Multiple sequence alignment was then performed using MAFFT, imposing E-INS-i model for multidomain proteins. IQ-TREE (Nguyen et al, 2015) was used to generate the phylogenetic tree and iTOL (Letunic & Bork, 2021) was used to visualize the tree.

**Coevolution Analysis**

Interspecies correlation serves as a good indicator to predict functional relationship between proteins. Other than *Dip2* and *PKC1*, a set of conserved housekeeping genes (*GAPDH, PGK1, ACT1, HSP60, CYTC, TPI1, CDC42, RPL5*) and known lipid metabolizing enzymes (*Dga1, Dgk1, Lro1, Tgl3, Faa1, Lcb1, Erg4*) were taken as control proteins. The obtained alignment was checked in JalView and arranged alphabetically to maintain homogeneity in comparison. This output alignment file was used to calculate pairwise genetic distances in MEGA X using bootstrap (1000 repetitions), employing the JTT model (Jones-Taylor Thornton model) and uniform mutation rates that represent the number of substitutions per site between two homologous proteins.

The obtained genetic distances were exported as a distance matrix and Pearson correlation coefficient was calculated using the following equation-

$$r = \frac{\sum_{i=1}^{n}(R_i-\bar{R})(S_i-\bar{S})}{\sqrt{\sum_{i=1}^{n}(R_i-\bar{R})^2}\sqrt{\sum_{i=1}^{n}(S_i-\bar{S})^2}}$$

The correlation coefficients were converted to normally distributed metric using Fisher's *r* to *z* transformation,

$$r' = \frac{1}{2} ln \left|\frac{1+r}{1-r}\right|$$

where,

$r$ = Pearson correlation coefficient

$r'$ = Fisher-transformed correlation coefficient

These transformed coefficients (r′) were further compared to generate z score/z test statistic using the given equation,

$$z = \frac{r_1' - r_2'}{\sqrt{\frac{1}{N_1-3} + \frac{1}{N_2-3}}}$$

where,

$r'_1$ is the first Fisher-transformed correlation coefficient

$r'_2$ is the second Fisher-transformed correlation coefficient

$N_1$ and $N_2$ denote the number of common organisms in the first and second correlation respectively. z-scores were calculated for all pairs where $r'_1$, representing Dip2-PKC correlation coefficient and $r'_2$ representing correlation coefficient for Dip2 with other protein controls, giving negative values for higher correlations and positive for lower ones. p-values were calculated from the obtained z-scores.

Patristic distance is the sum of the lengths of the branches that link two terminal nodes in a tree, denoting the divergence between the two nodes. Using the same collected sequences, phylogenetic trees were constructed by standard methods- Bayesian Inference, Maximum Likelihood (using JTT model), Neighbor Joining (NJ) and Minimum Evolution. Patristic distances were calculated for each phylogenetic model using PATRISTIC software and correlation coefficients were generated from the obtained distance matrices. Similar

phylogenetic patterns were observed where the homogeneity in correlation coefficient is maintained. Basically, a higher correlation score represents a stronger relationship between the rate at which the two proteins have evolved along the multiple branches of their phylogenetic trees.

**Statistical analysis**

All the statistical analyses were performed in Microsoft Excel and GraphPad Prism 9.3.1 (471). Statistical analysis of the differences between two groups was performed using a two-tailed, unpaired and parametric, Student's t-test. Error bars represent standard deviations (SD), except for lipidomic analyses, where error bars are plotted as standard error of mean (SEM). Significance of differences are marked based on the p-value obtained. *$p < 0.05$; **$p < 0.01$; ***$p < 0.001$; ****$p < 0.0001$; ns, not significant. All the experiments are replicated minimally thrice with technical replicates.

**Acknowledgement:**

We thank Dr. Krishnaveni Mishra (University of Hyderabad) and Dr. Purusharth I. Rajyaguru (Indian Institute of Science) for sharing yeast knockout strains with us. We thank Dr. Kaustuv Sanyal and Kuladeep Das (Jawaharlal Nehru Centre for Advanced Scientific Research) for generating *Δpsi1Δdip2* strain for us. We thank Dr. Sriram Varahan (CSIR-CCMB) for engaging discussions and sharing resources. We thank Saddam Shekh and Aakash Chandramouli for technical assistance with the LCMS experiments at IISER Pune. SS thanks University Grants Commission, India; SM and AC thank Council of Scientific and Industrial Research (CSIR), India, for the research fellowship. RSN thanks healthcare theme projects-

Fundamental and Innovative CSIR in Science of Tomorrow (FIRST; MLP-0162) and Niche Creation Project (NCP; MLP-0138) of CSIR, India; J.C. Bose Fellowship of SERB, India; and Centre of Excellence Project of Department of Biotechnology, India. SSK thanks Swarnajayanti Fellowship from the Science and Engineering Research Board (SERB), Department of Science and Technology (DST), Government of India (Grant number SB/SJF/2021-22/01) and the Department of Science & Technology–Funds for Improvement of S&T Infrastructure Development (DST-FIST) (grant number SR/FST/LSII-043/2016) to the Department of Biology, IISER Pune for setting up the Biological Mass Spectrometry Facility.

**References:**

1. Abhyankar V, Kaduskar B, Kamat SS, Deobagkar D, Ratnaparkhi GS (2018) Drosophila DNA/RNA methyltransferase contributes to robust host defense in aging animals by regulating sphingolipid metabolism. *J Exp Biol* 221
2. Adeyo O, Horn PJ, Lee S, Binns DD, Chandrahas A, Chapman KD, Goodman JM (2011) The yeast lipin orthologue Pah1p is important for biogenesis of lipid droplets. *J Cell Biol* 192: 1043-1055
3. Altschul SF, Gish W, Miller W, Myers EW, Lipman DJ (1990) Basic local alignment search tool. *J Mol Biol* 215: 403-410
4. Antonsson B, Montessuit S, Friedli L, Payton MA, Paravicini G (1994) Protein kinase C in yeast. Characteristics of the Saccharomyces cerevisiae PKC1 gene product. *J Biol Chem* 269: 16821-16828
5. Banfic H, Bedalov A, York JD, Visnjic D (2013) Inositol pyrophosphates modulate S phase progression after pheromone-induced arrest in Saccharomyces cerevisiae. *J Biol Chem* 288: 1717-1725

6. Bass D, Czech L, Williams BAP, Berney C, Dunthorn M, Mahe F, Torruella G, Stentiford GD, Williams TA (2018) Clarifying the Relationships between Microsporidia and Cryptomycota. *J Eukaryot Microbiol* 65: 773-782
7. Brachmann CB, Davies A, Cost GJ, Caputo E, Li J, Hieter P, Boeke JD (1998) Designer deletion strains derived from Saccharomyces cerevisiae S288C: a useful set of strains and plasmids for PCR-mediated gene disruption and other applications. *Yeast* 14: 115-132
8. Breslow DK, Collins SR, Bodenmiller B, Aebersold R, Simons K, Shevchenko A, Ejsing CS, Weissman JS (2010) Orm family proteins mediate sphingolipid homeostasis. *Nature* 463: 1048-1053
9. Calabrese B, Halpain S (2005) Essential role for the PKC target MARCKS in maintaining dendritic spine morphology. *Neuron* 48: 77-90
10. Carrasco S, Merida I (2007) Diacylglycerol, when simplicity becomes complex. *Trends Biochem Sci* 32: 27-36
11. Colon-Gonzalez F, Kazanietz MG (2006) C1 domains exposed: from diacylglycerol binding to protein-protein interactions. *Biochim Biophys Acta* 1761: 827-837
12. Denis V, Cyert MS (2005) Molecular analysis reveals localization of Saccharomyces cerevisiae protein kinase C to sites of polarized growth and Pkc1p targeting to the nucleus and mitotic spindle. *Eukaryot Cell* 4: 36-45
13. Dey P, Su WM, Han GS, Carman GM (2017) Phosphorylation of lipid metabolic enzymes by yeast protein kinase C requires phosphatidylserine and diacylglycerol. *J Lipid Res* 58: 742-751
14. Doignon F, Laquel P, Testet E, Tuphile K, Fouillen L, Bessoule JJ (2016) Requirement of Phosphoinositides Containing Stearic Acid To Control Cell Polarity. *Mol Cell Biol* 36: 765-780
15. Edgar RS, Green EW, Zhao Y, van Ooijen G, Olmedo M, Qin X, Xu Y, Pan M, Valekunja UK, Feeney KA *et al* (2012) Peroxiredoxins are conserved markers of circadian rhythms. *Nature* 485: 459-464
16. Eichmann TO, Lass A (2015) DAG tales: the multiple faces of diacylglycerol--stereochemistry, metabolism, and signaling. *Cell Mol Life Sci* 72: 3931-3952

17. Etcheberrigaray R, Tan M, Dewachter I, Kuiperi C, Van der Auwera I, Wera S, Qiao L, Bank B, Nelson TJ, Kozikowski AP *et al* (2004) Therapeutic effects of PKC activators in Alzheimer's disease transgenic mice. *Proc Natl Acad Sci U S A* 101: 11141-11146
18. Fourment M, Gibbs MJ (2006) PATRISTIC: a program for calculating patristic distances and graphically comparing the components of genetic change. *BMC Evol Biol* 6: 1
19. Gietz RD, Schiestl RH (2007) High-efficiency yeast transformation using the LiAc/SS carrier DNA/PEG method. *Nat Protoc* 2: 31-34
20. Goldberg JM, Manning G, Liu A, Fey P, Pilcher KE, Xu Y, Smith JL (2006) The dictyostelium kinome--analysis of the protein kinases from a simple model organism. *PLoS Genet* 2: e38
21. Heinisch JJ, Rodicio R (2018) Protein kinase C in fungi-more than just cell wall integrity. *FEMS Microbiol Rev* 42
22. Hurley JH, Newton AC, Parker PJ, Blumberg PM, Nishizuka Y (1997) Taxonomy and function of C1 protein kinase C homology domains. *Protein Sci* 6: 477-480
23. Jacoby JJ, Schmitz HP, Heinisch JJ (1997) Mutants affected in the putative diacylglycerol binding site of yeast protein kinase C. *FEBS Lett* 417: 219-222
24. Jain K, Basu A (2014) Protein Kinase C-epsilon Promotes EMT in Breast Cancer. *Breast Cancer (Auckl)* 8: 61-67
25. James TY, Pelin A, Bonen L, Ahrendt S, Sain D, Corradi N, Stajich JE (2013) Shared signatures of parasitism and phylogenomics unite Cryptomycota and microsporidia. *Curr Biol* 23: 1548-1553
26. Jun Y, Fratti RA, Wickner W (2004) Diacylglycerol and its formation by phospholipase C regulate Rab- and SNARE-dependent yeast vacuole fusion. *J Biol Chem* 279: 53186-53195
27. Keenan C, Phillips P, Thio M, Pears C (1997) Protein kinase C in dictyostelium discoideum. *Biochem Soc Trans* 25: S592
28. Kelkar DS, Ravikumar G, Mehendale N, Singh S, Joshi A, Sharma AK, Mhetre A, Rajendran A, Chakrapani H, Kamat SS (2019) A chemical-genetic screen identifies ABHD12 as an oxidized-phosphatidylserine lipase. *Nat Chem Biol* 15: 169-178

29. Kishimoto A, Takai Y, Mori T, Kikkawa U, Nishizuka Y (1980) Activation of calcium and phospholipid-dependent protein kinase by diacylglycerol, its possible relation to phosphatidylinositol turnover. *J Biol Chem* 255: 2273-2276
30. Kumar M, Ojha S, Rai P, Joshi A, Kamat SS, Mallik R (2019) Insulin activates intracellular transport of lipid droplets to release triglycerides from the liver. *J Cell Biol* 218: 3697-3713
31. LaFayette SL, Collins C, Zaas AK, Schell WA, Betancourt-Quiroz M, Gunatilaka AA, Perfect JR, Cowen LE (2010) PKC signaling regulates drug resistance of the fungal pathogen Candida albicans via circuitry comprised of Mkc1, calcineurin, and Hsp90. *PLoS Pathog* 6: e1001069
32. Larsson C, Ali MA, Pandzic T, Lindroth AM, He L, Sjoblom T (2017) Loss of Dip2C in RKO cells stimulates changes in DNA methylation and epithelial-mesenchymal transition. *BMC Cancer* 17: 487
33. Larsson E, Hubert M, Lundmark R (2020) Analysis of Protein and Lipid Interactions Using Liposome Co-sedimentation Assays. *Methods Mol Biol* 2169: 119-127
34. Le Guedard M, Bessoule JJ, Boyer V, Ayciriex S, Velours G, Kulik W, Ejsing CS, Shevchenko A, Coulon D, Lessire R *et al* (2009) PSI1 is responsible for the stearic acid enrichment that is characteristic of phosphatidylinositol in yeast. *FEBS J* 276: 6412-6424
35. Lee KS, Irie K, Gotoh Y, Watanabe Y, Araki H, Nishida E, Matsumoto K, Levin DE (1993) A yeast mitogen-activated protein kinase homolog (Mpk1p) mediates signalling by protein kinase C. *Mol Cell Biol* 13: 3067-3075
36. Levin DE (2005) Cell wall integrity signaling in Saccharomyces cerevisiae. *Microbiol Mol Biol Rev* 69: 262-291
37. Li D, Yang SG, He CW, Zhang ZT, Liang Y, Li H, Zhu J, Su X, Gong Q, Xie Z (2020) Excess diacylglycerol at the endoplasmic reticulum disrupts endomembrane homeostasis and autophagy. *BMC Biol* 18: 107
38. Li J, Ping JL, Ma B, Chen YR, Li LQ (2017) Dip2C expression in breast cancer and its clinical significance. *Pathol Res Pract* 213: 1394-1399

39. Liu T, Shi Y, Chan MTV, Peng G, Zhang Q, Sun X, Zhu Z, Xie Y, Sham KWY, Li J *et al* (2018) Developmental protein kinase C hyper-activation results in microcephaly and behavioral abnormalities in zebrafish. *Transl Psychiatry* 8: 232
40. Lu S, Wang J, Chitsaz F, Derbyshire MK, Geer RC, Gonzales NR, Gwadz M, Hurwitz DI, Marchler GH, Song JS *et al* (2020) CDD/SPARCLE: the conserved domain database in 2020. *Nucleic Acids Res* 48: D265-D268
41. Lu SW, Kroken S, Lee BN, Robbertse B, Churchill AC, Yoder OC, Turgeon BG (2003) A novel class of gene controlling virulence in plant pathogenic ascomycete fungi. *Proc Natl Acad Sci U S A* 100: 5980-5985
42. Ma J, Zhang LQ, He ZX, He XX, Wang YJ, Jian YL, Wang X, Zhang BB, Su C, Lu J *et al* (2019) Autism candidate gene Dip2A regulates spine morphogenesis via acetylation of cortactin. *PLoS Biol* 17: e3000461
43. Marignani PA, Epand RM, Sebaldt RJ (1996) Acyl chain dependence of diacylglycerol activation of protein kinase C activity in vitro. *Biochem Biophys Res Commun* 225: 469-473
44. Marrocco V, Bogomolovas J, Ehler E, Dos Remedios CG, Yu J, Gao C, Lange S (2019) PKC and PKN in heart disease. *J Mol Cell Cardiol* 128: 212-226
45. Milne SB, Ivanova PT, Armstrong MD, Myers DS, Lubarda J, Shulga YV, Topham MK, Brown HA, Epand RM (2008) Dramatic differences in the roles in lipid metabolism of two isoforms of diacylglycerol kinase. *Biochemistry* 47: 9372-9379
46. Mondal S, Kinatukara P, Singh S, Shambhavi S, Patil GS, Dubey N, Singh SH, Pal B, Shekar PC, Kamat SS *et al* (2022) Dip2 is a unique regulator of diacylglycerol lipid homeostasis in eukaryotes. *Elife* 11
47. Mori T, Takai Y, Yu B, Takahashi J, Nishizuka Y, Fujikura T (1982) Specificity of the fatty acyl moieties of diacylglycerol for the activation of calcium-activated, phospholipid-dependent protein kinase. *J Biochem* 91: 427-431
48. Morlock KR, McLaughlin JJ, Lin YP, Carman GM (1991) Phosphatidate phosphatase from Saccharomyces cerevisiae. Isolation of 45- and 104-kDa forms of the enzyme that are differentially regulated by inositol. *J Biol Chem* 266: 3586-3593

49. Narra HP, Shubitz LF, Mandel MA, Trinh HT, Griffin K, Buntzman AS, Frelinger JA, Galgiani JN, Orbach MJ (2016) A Coccidioides posadasii CPS1 Deletion Mutant Is Avirulent and Protects Mice from Lethal Infection. *Infect Immun* 84: 3007-3016
50. Newton AC (2018) Protein kinase C: perfectly balanced. *Crit Rev Biochem Mol Biol* 53: 208-230
51. Nguyen LT, Schmidt HA, von Haeseler A, Minh BQ (2015) IQ-TREE: a fast and effective stochastic algorithm for estimating maximum-likelihood phylogenies. *Mol Biol Evol* 32: 268-274
52. Nishizuka Y (1984) The role of protein kinase C in cell surface signal transduction and tumour promotion. *Nature* 308: 693-698
53. Nitta Y, Yamazaki D, Sugie A, Hiroi M, Tabata T (2017) DISCO Interacting Protein 2 regulates axonal bifurcation and guidance of Drosophila mushroom body neurons. *Dev Biol* 421: 233-244
54. Nomura W, Inoue Y (2015) Methylglyoxal activates the target of rapamycin complex 2-protein kinase C signaling pathway in Saccharomyces cerevisiae. *Mol Cell Biol* 35: 1269-1280
55. Ocana-Pallares E, Williams TA, Lopez-Escardo D, Arroyo AS, Pathmanathan JS, Bapteste E, Tikhonenkov DV, Keeling PJ, Szollosi GJ, Ruiz-Trillo I (2022) Divergent genomic trajectories predate the origin of animals and fungi. *Nature* 609: 747-753
56. Ochoa D, Pazos F (2014) Practical aspects of protein co-evolution. *Front Cell Dev Biol* 2: 14
57. Pathak D, Mehendale N, Singh S, Mallik R, Kamat SS (2018) Lipidomics Suggests a New Role for Ceramide Synthase in Phagocytosis. *ACS Chem Biol* 13: 2280-2287
58. Patil GS, Kinatukara P, Mondal S, Shambhavi S, Patel KD, Pramanik S, Dubey N, Narasimhan S, Madduri MK, Pal B *et al* (2021) A universal pocket in Fatty acyl-AMP ligases ensures redirection of fatty acid pool away from Coenzyme A-based activation. *Elife* 10
59. Pazos F, Valencia A (2001) Similarity of phylogenetic trees as indicator of protein-protein interaction. *Protein Eng* 14: 609-614

60. Philippi A, Roschmann E, Tores F, Lindenbaum P, Benajou A, Germain-Leclerc L, Marcaillou C, Fontaine K, Vanpeene M, Roy S *et al* (2005) Haplotypes in the gene encoding protein kinase c-beta (PRKCB1) on chromosome 16 are associated with autism. *Mol Psychiatry* 10: 950-960
61. Reyland ME (2009) Protein kinase C isoforms: Multi-functional regulators of cell life and death. *Front Biosci (Landmark Ed)* 14: 2386-2399
62. Rockenfeller P, Smolnig M, Diessl J, Bashir M, Schmiedhofer V, Knittelfelder O, Ring J, Franz J, Foessl I, Khan MJ *et al* (2018) Diacylglycerol triggers Rim101 pathway-dependent necrosis in yeast: a model for lipotoxicity. *Cell Death Differ* 25: 767-783
63. Roncero C, Duran A (1985) Effect of Calcofluor white and Congo red on fungal cell wall morphogenesis: in vivo activation of chitin polymerization. *J Bacteriol* 163: 1180-1185
64. Rosse C, Linch M, Kermorgant S, Cameron AJ, Boeckeler K, Parker PJ (2010) PKC and the control of localized signal dynamics. *Nat Rev Mol Cell Biol* 11: 103-112
65. Sasser T, Qiu QS, Karunakaran S, Padolina M, Reyes A, Flood B, Smith S, Gonzales C, Fratti RA (2012) Yeast lipin 1 orthologue pah1p regulates vacuole homeostasis and membrane fusion. *J Biol Chem* 287: 2221-2236
66. Schmitz-Peiffer C, Biden TJ (2008) Protein kinase C function in muscle, liver, and beta-cells and its therapeutic implications for type 2 diabetes. *Diabetes* 57: 1774-1783
67. Schmitz HP, Heinisch JJ (2003) Evolution, biochemistry and genetics of protein kinase C in fungi. *Curr Genet* 43: 245-254
68. Schmitz HP, Lorberg A, Heinisch JJ (2002) Regulation of yeast protein kinase C activity by interaction with the small GTPase Rho1p through its amino-terminal HR1 domain. *Mol Microbiol* 44: 829-840
69. Schuhmacher M, Grasskamp AT, Barahtjan P, Wagner N, Lombardot B, Schuhmacher JS, Sala P, Lohmann A, Henry I, Shevchenko A *et al* (2020) Live-cell lipid biochemistry reveals a role of diacylglycerol side-chain composition for cellular lipid dynamics and protein affinities. *Proc Natl Acad Sci U S A* 117: 7729-7738
70. Starr ML, Hurst LR, Fratti RA (2016) Phosphatidic Acid Sequesters Sec18p from cis-SNARE Complexes to Inhibit Priming. *Traffic* 17: 1091-1109

71. Sussman A, Huss K, Chio LC, Heidler S, Shaw M, Ma D, Zhu G, Campbell RM, Park TS, Kulanthaivel P *et al* (2004) Discovery of cercosporamide, a known antifungal natural product, as a selective Pkc1 kinase inhibitor through high-throughput screening. *Eukaryot Cell* 3: 932-943

72. Wang Y, He D, Chu Y, Zuo YS, Xu XW, Chen XL, Zhao WS, Zhang Y, Yang J, Peng YL (2016) MoCps1 is important for conidiation, conidial morphology and virulence in Magnaporthe oryzae. *Curr Genet* 62: 861-871

73. Wang Y, Rubin H, Ravid S (1996) Dictyostelium protein kinase C-delta-like protein is localized in the cell nucleus. *Biol Cell* 86: 103-109

74. Yang C, Kazanietz MG (2003) Divergence and complexities in DAG signaling: looking beyond PKC. *Trends Pharmacol Sci* 24: 602-608

75. Yofe I, Schuldiner M (2014) Primers-4-Yeast: a comprehensive web tool for planning primers for Saccharomyces cerevisiae. *Yeast* 31: 77-80

76. Zhang B, Li Z, Zhang R, Hu Y, Jiang Y, Cao T, Wang J, Gong L, Ji L, Mu H *et al* (2019) PKCgamma promotes axonal remodeling in the cortico-spinal tract via GSK3beta/beta-catenin signaling after traumatic brain injury. *Sci Rep* 9: 17078

77. Kamiya, Y., Mizuno, S., Komenoi, S., Sakai, H., & Sakane, F. (2016). Activation of conventional and novel protein kinase C isozymes by different diacylglycerol molecular species. *Biochemistry and Biophysics Reports*, *7*, 361–366. https://doi.org/10.1016/j.bbrep.2016.07.017

78. Letunic, I., & Bork, P. (2021). Interactive Tree Of Life (iTOL) v5: An online tool for phylogenetic tree display and annotation. *Nucleic Acids Research*, *49*(W1), W293–W296. https://doi.org/10.1093/nar/gkab301

79. Masayoshi, G., Sekiguchi, K., Nomura, H., Kikkawa, U., & Nishizuka, Y. (1987). Further studies on the specificity of diacylglycerol for protein kinase C activation. *Biochemical and*

*Biophysical Research Communications*, *144*(2), 598–605. https://doi.org/10.1016/S0006-291X(87)80008-6

80. Saiz-Baggetto, S., Dolz-Edo, L., Méndez, E., García-Bolufer, P., Marí, M., Bañó, M. C., Fariñas, I., Morante-Redolat, J. M., Igual, J. C., & Quilis, I. (2023). A Multimodel Study of the Role of Novel PKC Isoforms in the DNA Integrity Checkpoint. *International Journal of Molecular Sciences*, *24*(21), 15796. https://doi.org/10.3390/ijms242115796

81. Sariki, S. K., Kumawat, R., Singh, V., & Tomar, R. S. (2019). Flocculation of *Saccharomyces cerevisiae* is dependent on activation of Slt2 and Rlm1 regulated by the cell wall integrity pathway. *Molecular Microbiology*, *112*(4), 1350–1369. https://doi.org/10.1111/mmi.14375

## Main Figures:

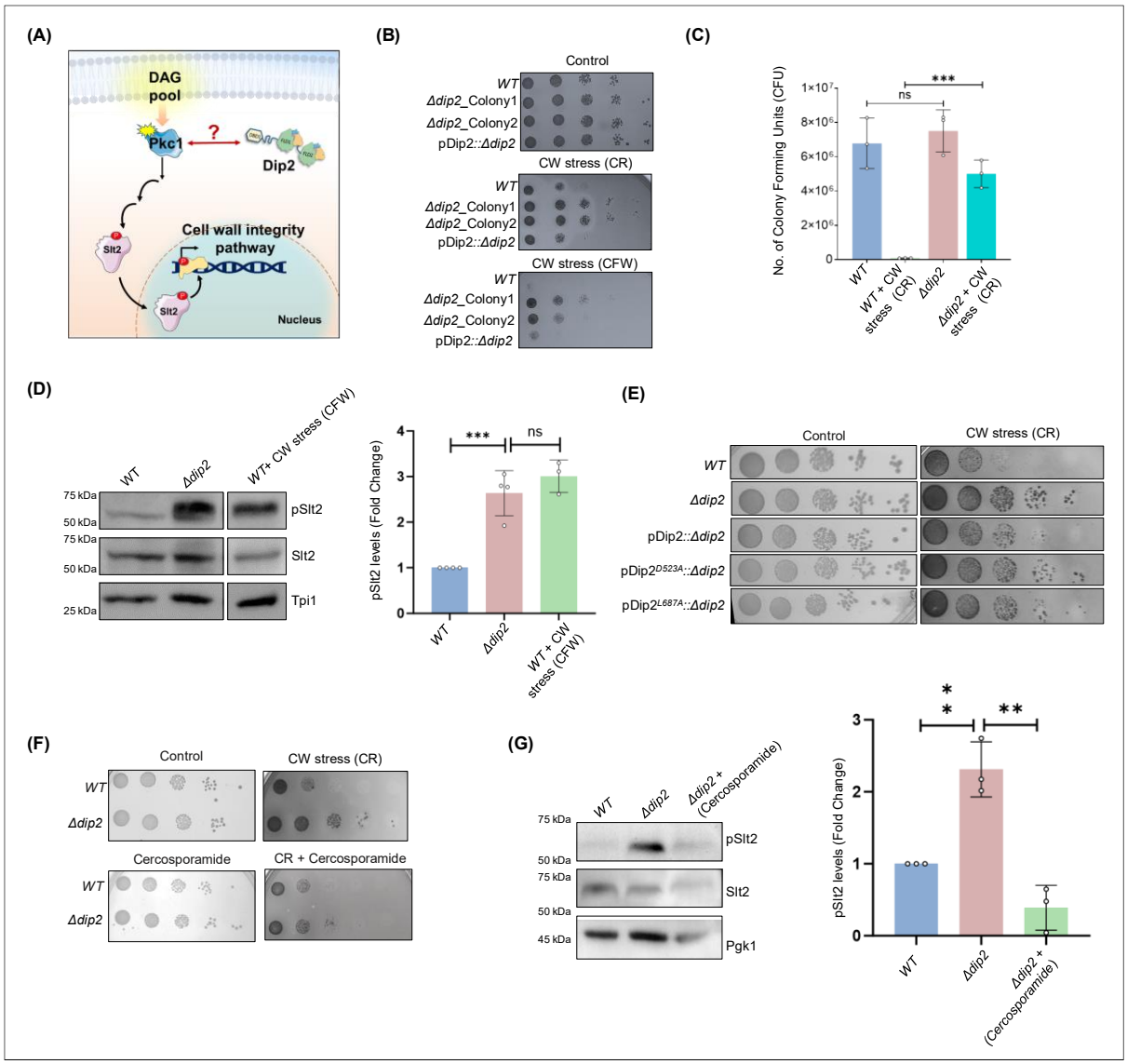


**Figure 1. Deletion of Dip2 leads to increased cell wall stress resistance.**

(**A**) A model depicting the possible role of Dip2 in regulating DAG species required for PKC activation which governs the CWI pathway in yeast by activating the downstream MAPK cascade. Activation of the MAPK cascade results in increased cell wall synthesis thereby strengthening the cell wall. Dip2 has been depicted in its three-domain architecture, harbouring DMAP-binding domain 1 (DBD1), tandem fatty acyl-AMP ligase-like domains (FLD1 and FLD2).

(**B**) Serial dilution assay for *WT*, two biological replicates of *Δdip2* (*Δdip2*_Colony1 and *Δdip2*_Colony2; *Δdip2*_Colony1 has been used for further experiments). pDip2*::Δdip2* represents *Δdip2*_Colony1 complemented with Dip2 expressed under its native promoter. Control plate contains synthetic complete (SC) media and cell wall (CW) stress plate has either congo red (CR) (100µg/mL) or calcofluor white (CFW) (50µg/mL). N=3.

(**C**) Colony forming units of *WT* and *Δdip2* grown in SC media control and cell wall stress induced by CR (100µg/mL). Data are represented as mean ± SD (unpaired, two-tailed Student's t-test; n = 3; ***p < 0.001; ns = not significant). N=3.

(**D**) Representative western blot showing pSlt2 (56 kDa) levels in *WT* and *Δdip2* compared to the *WT* treated with CFW for 30 min, used as a positive control. Bar graph showing quantification of fold change in the pSlt2 levels, normalised with total Slt2. Triose phosphate isomerase (Tpi1) (27 kDa) has been used as a loading control. Data are represented as mean ± SD (unpaired, two-tailed Student's t-test; *n* > 3; ***p < 0.001; ns = not significant.

**(E)** Serial dilution assay image in synthetic complete (SC) media control plate and in the presence of congo red (100µg/mL) for *WT* and *Δdip2* compared with *Δdip2* complemented with wildtype and catalytically inactive Dip2 mutants ($Dip2^{D523A}$ and $Dip2^{L687A}$), expressed in a plasmid pYSM7, under its native promoter. N=3.

**(F)** Serial dilution assay for *WT* and *Δdip2* grown in SD media control and in the presence of CR (100µg/mL) and cercosporamide (2µg/mL). N=3.

**(G)** Representative western blot for *WT*, *Δdip2* and cercosporamide treated *Δdip2* showing the levels of pslt2 (56 kDa). Quantification of pSlt2 levels for *Δdip2* treated with cercosporamide (5µg/mL) compared to *WT* and *Δdip2* control, normalised with total Slt2. Phosphoglycerate

kinase (Pgk1) (45 kDa) has been used as a loading control. Data are represented as mean ± SD (unpaired, two-tailed Student's t-test; *N*=3; **p < 0.01; ns = not significant).

The online version of this article includes the following source data and figure supplement(s) for figure 1:

**Figure 1 - Source data 1-1B:** Spot assay for WT, *Δdip2* and pDip2*::Δdip2* under cell wall stress.

**Figure 1 - Source data 2-1C:** Quantification of CFU for WT and *Δdip2* in the presence of CR.

**Figure 1 - Source data 3-1D:** Western blot and quantification for WT, *Δdip2* and WT treated with CFW.

**Figure 1 - Source data 4-1E:** Spot assay for the catalytic mutants of Dip2

**Figure 1 - Source data 5-1F:** Spot assay for WT, *Δdip2* in the presence of CR and cercosporamide.

**Figure 1 - Source data 6-1G:** Western blot and quantification for WT, *Δdip2* and *Δdip2* treated with cercosporamide.

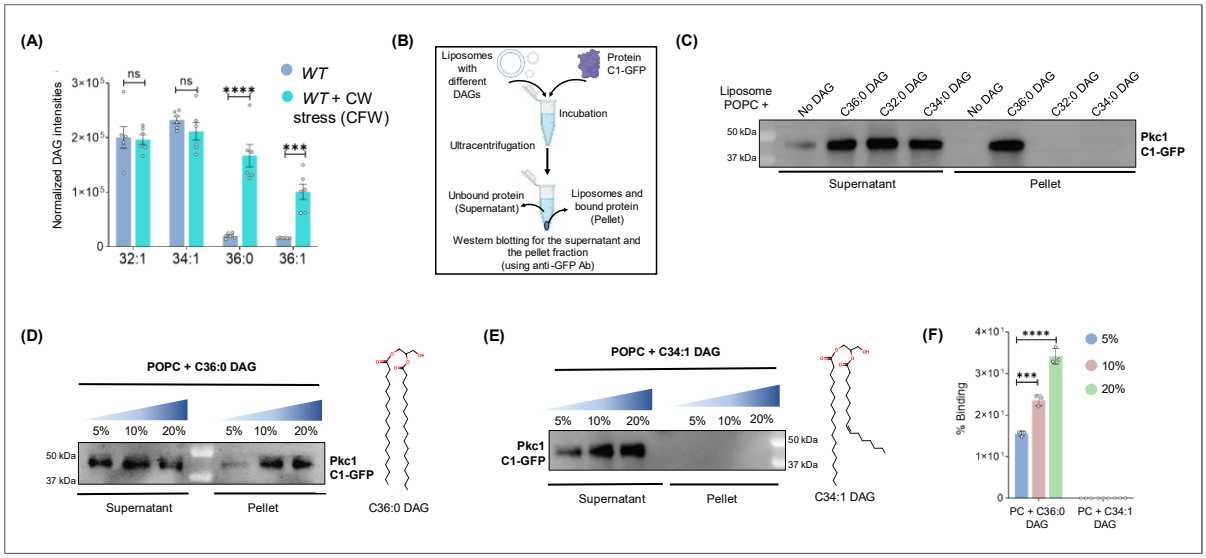


**Figure 2. Dip2-regulated selective DAG subspecies are associated with the activation of PKC signalling.**

(**A**) Lipidomic analysis of *WT* treated with CFW (50µg/mL) for 30 minutes. DAG intensities normalized to the total protein content in *WT*+CFW have been compared to the intensities from the same species in *WT* control sample. Data are represented as mean ± standard error of mean (SEM) (unpaired, two-tailed Student's t-test; N=6). ****p < 0.0001; ***p < 0.001 ns = not significant.

(**B**) A flowchart for the liposome sedimentation assay explaining the incubation of liposomes with protein, followed by ultracentrifugation and western blotting for supernatant (unbound protein) and pellet (bound protein) fraction.

**(C)** Representative western blot for liposome sedimentation assay with different DAGs showing supernatant fraction (unbound protein) and pellet fraction (liposome bound protein), probed for C1 domain using anti-GFP antibody (43k Da). N > 3.

**(D)** Western blot probing for C1 domain bound to different concentrations of C36:0 DAG containing liposomes (pellet fraction) and the unbound protein (supernatant fraction) using anti GFP antibody. Structure of respective DAGs is shown on the right side. N > 3.

**(E)** Western blot probing for C1 domain at different concentrations of C34:1 DAG containing liposomes in both pellet and supernatant fractions. Structure of respective DAGs have been shown on the right side. N > 3.

**(F)** Bar graph showing quantification of percentage binding of C1-GFP with increasing concentrations of specific (C36:0) and non-specific (C34:1) DAGs. Data are represented as mean ± SD (unpaired, two-tailed Student's t-test; *n*=3; ***p < 0.001; ns = not significant), N=3.

The online version of this article includes the following source data and figure supplement(s) for figure 2:

**Figure 2 - Source data 1- 2B:** Quantification of DAGs in WT and CFW treated WT.

**Figure 2 - Source data 2- 2C:** Western blot for C1-GFP incubated with different DAGs containing liposomes.

**Figure 2 - Source data 3- 2D:** Western blot for C1-GFP incubated C36:0 DAGs containing liposomes.

**Figure 2 - Source data 4- 2E:** Western blot for C1-GFP incubated C34:1 DAGs containing liposomes.

**Figure 2 - Source data 5- 2F:** Quantification for percent binding of C1 domain with C36:0 and C34:1 DAGs containing liposomes.

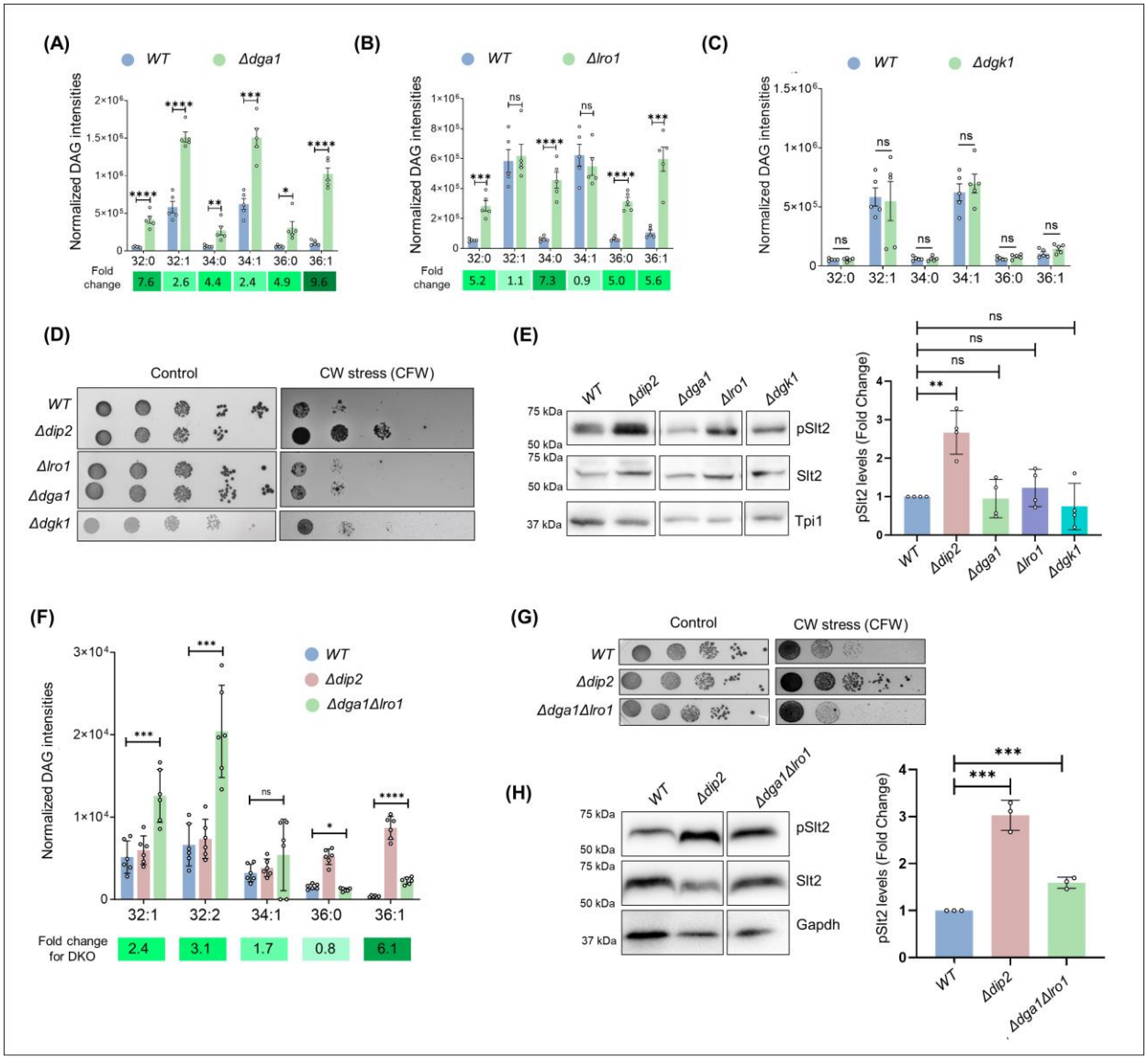


**Figure 3. PKC activation is independent of bulk DAG metabolism pathway.**

(**A-C**) Lipidomic analysis of DAGs in *Δdga1*, *Δlro1* and *Δdgk1*, compared to *WT*. Fold change values are mentioned below and are represented as green colour gradient. Data are represented as mean ± SEM (unpaired, two-tailed Student's t-test; N = 5) ****p < 0.0001; ***p < 0.001; **p < 0.01; *p < 0.05; ns = not significant.

(**D**) Serial dilution assay for single knockouts of bulk DAG acting enzymes (Dga1, Lro1 and Dgk1) in the presence of CFW (50µg/mL), compared to SC media control plate. N=3.

(**E)** Representative western blot and quantification of pSlt2 (56 kDa) levels in deletion strains of DAG metabolizing enzymes. Fold change has been quantified with respect to the total Slt2. Triose phosphate isomerase (Tpi1) (27 kDa) has been used as a loading control. Data are represented as mean ± SD (unpaired, two-tailed Student's t-test); N=4; ****p < 0.0001; *p < 0.05; ns = not significant.

**(F)** DAG subspecies quantification using lipidomics for the double knockout of *LRO1* and *DGA1*, compared to *WT* and *Δdip2*. Data are represented as mean ± SEM (unpaired, two-tailed Student's t-test); n = 6; ****p < 0.0001; ***p < 0.00; *p < 0.05; ns = not significant.

**(G)** Serial dilution assay image for the cell wall stress sensitivity of *Δdga1Δlro1,* compared to *WT* and *Δdip2*, in the presence of CFW (50µg/mL), compared to SC media control plate. N=3. SC media control image is reused in Figure 3- figure supplement 2.

**(H)** Representative western blot for pSlt2 (56 kDa) estimation in *Δdga1Δlro1,* compared to total Slt2 and a loading control Glyceraldehyde-3-phosphate dehydrogenase (Gapdh) (36 kDa). Fold change has been quantified with respect to the total Slt2. Data are represented as mean ± SD (unpaired, two-tailed Student's t-test); N=3; **p < 0.01; ns = not significant.

The online version of this article includes the following source data and figure supplement(s) for figure 3:

**Figure 3 - Source data 1- 3A:** Quantification of DAG in *Δdga1*.

**Figure 3 - Source data 2- 3B:** Quantification of DAG in *Δlro1*.

**Figure 3 - Source data 3- 3C:** Quantification of DAG in *Δdgk1*.

**Figure 3 - Source data 4- 3D:** Spot assay for single knock outs of DAG acting enzymes.

**Figure 3 - Source data 5- 3E:** Western blots and quantification for single knockouts of DAG acting enzymes.

**Figure 3 - Source data 6- 3F:** DAG quantification for double knockouts of *LRO1* and *DGA1*.

**Figure 3 - Source data 7- 3G:** Spot assay for double knockouts of *LRO1* and *DGA1 in* the presence of CFW.

**Figure 3 - Source data 8- 3H:** Western blots and quantification of pSLt2 for double knockouts of *LRO1* and *DGA1*.

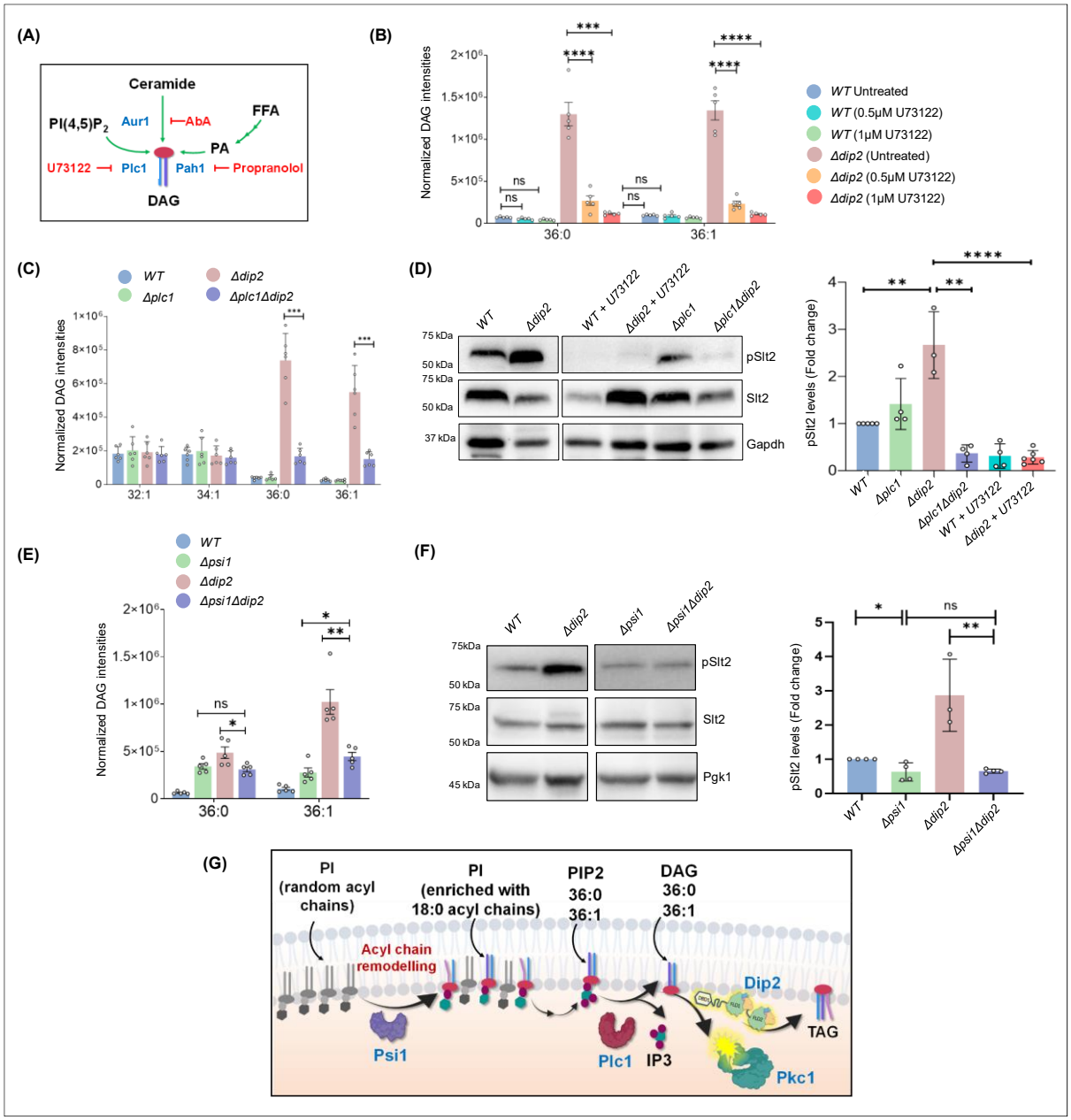


**Figure 4. Psi1-Plc1-Dip2 triad axis regulates selective DAG subspecies to modulate PKC signalling**.

**(A)** Schematic showing various pathways (green arrows) that feed into the production of DAGs in the presence of various enzymes (shown in blue) and different chemical inhibitors (red) blocking the respective pathways.

(**B**) Quantification of selective DAGs in *WT* and *Δdip2* samples treated with two different concentrations, i.e., 0.5 and 1 µM of U73122. Data are represented as mean ± SEM (unpaired, two-tailed Student's t-test; N = 5). ****p < 0.0001; ***p < 0.001; ns = not significant.

**(C)** Specific DAG quantification using lipidomics for deletion of *Δplc1* and *Δplc1Δdip2*. Data are represented as mean ± SEM (unpaired, two-tailed Student's t-test; n = 6). ****p < 0.0001; ***p < 0.001 ns = not significant. N=6.

(**D)** Representative western blot image and quantification of pSlt2 (56 kDa) levels for indicated samples. Fold change has been quantified with respect to the total Slt2. Gapdh (36 kDa) has been used as a loading control. Data are represented as mean ± SD (unpaired, two-tailed Student's t-test; N>4; ****p < 0.0001; **p < 0.01; ns = not significant.

(**E)** Lipidomic analysis of specific DAGs in double knockout of *PSI1* and *DIP2*, compared with *WT* and *Δpsi1*. Data are represented as mean ± SEM (unpaired, two-tailed Student's t-test; **p < 0.01; *p < 0.05; ns = not significant. N = 5).

**(F**) Representative western blot image and quantification of pSlt2 (56 kDa) levels for indicated samples. Two data points for controls (*WT* and *Δdip2*) are same as that of Figure 4D. Fold change has been quantified with respect to the total Slt2. Phosphoglycerate kinase (Pgk1) (45 kDa) has been used as a loading control. Data are represented as mean ± SD (unpaired, two-tailed Student's t-test; N>3; ****p < 0.0001; ***p < 0.001; ns = not significant.

(**G**) Schematic showing Psi1-Plc1-Dip2 axis to regulate Pkc1 signalling where Psi1 remodels phosphoinositides (PI) to enrich it with C36:0 and C36:1 containing acyl chain, which is channelled to the selective DAGs via Plc1 and in turn activate Pkc1.

The online version of this article includes the following source data and figure supplement(s) for figure 4:

**Figure 4 - Source data 1- 4B:** Quantification of DAG in WT and *Δdip2* in the presence of Plc1 inhibitor.

**Figure 4 - Source data 2- 4C:** Quantification of DAG in double knockout of *DIP2* and *PLC1*.

**Figure 4 - Source data 3- 4D:** Western blot and quantification of pSlt2 in the double knockout of *DIP2* and *PLC1* and in the presence of Plc1 inhibitor.

**Figure 4 - Source data 4- 4E:** Quantification of DAG in double knockout of *DIP2* and *PSI1*.

**Figure 4 - Source data 5- 4F:** Western blot and quantification of pSlt2 in the double knockout of *DIP2* and *PSI1*.

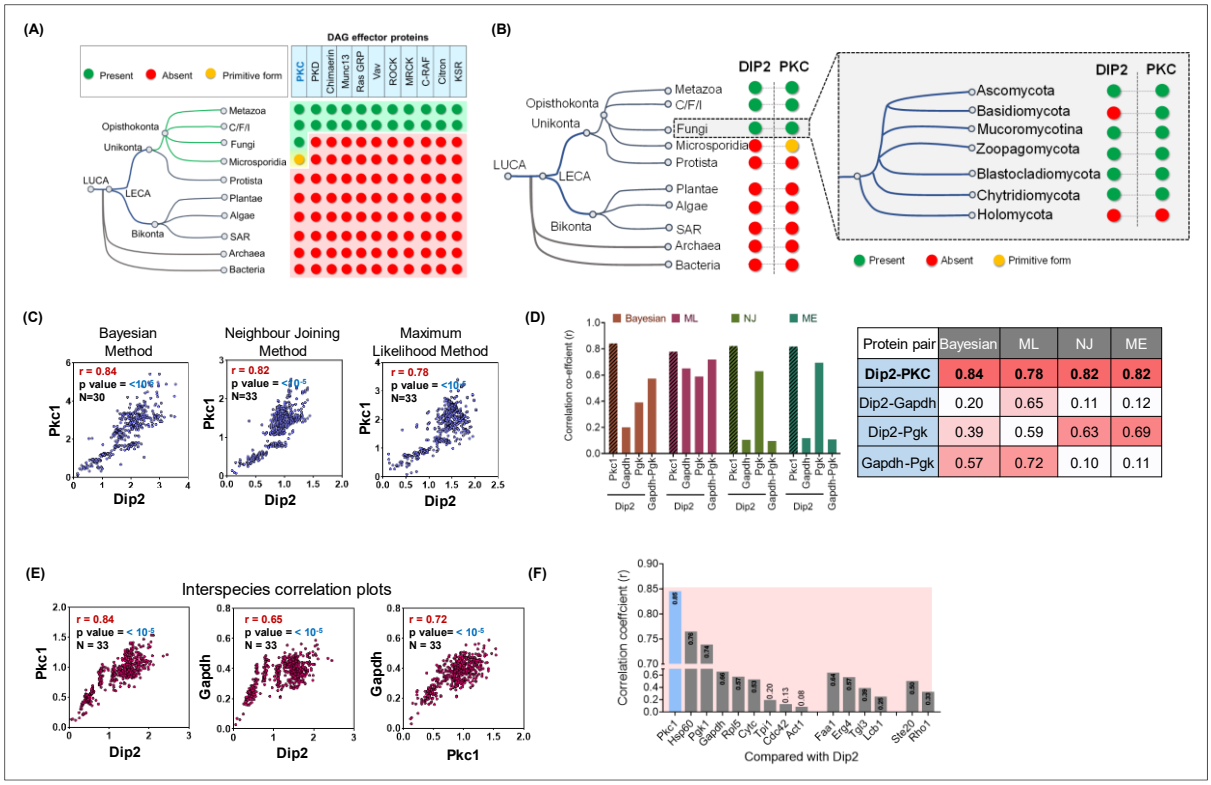


| Protein pair | Bayesian | ML | NJ | ME |
|---|---|---|---|---|
| **Dip2-PKC** | **0.84** | **0.78** | **0.82** | **0.82** |
| Dip2-Gapdh | 0.20 | 0.65 | 0.11 | 0.12 |
| Dip2-Pgk | 0.39 | 0.59 | 0.63 | 0.69 |
| Gapdh-Pgk | 0.57 | 0.72 | 0.10 | 0.11 |

**Figure 5. Dip2 and PKC share a parallel history of co-emergence coevolution across Opisthokonta.**

(**A**) Emergence and distribution of DAG effector proteins across tree of life. Green circles represent presence, while red circles represent absence of effector proteins. Yellow circle represents the primitive form of PKC. List of DAG effectors is taken from a previous study (Colon-Gonzalez & Kazanietz, 2006).

(**B**) Phylogenetic profiling of Dip2 and PKC shows their co-emergence in Opisthokonta. Inset shows presence of Dip2 and PKC in different fungal branches (Ocana-Pallares et al., 2022). Green circle represents presence, red represents absence, while yellow circle represents a primitive form of PKC harbouring only C1 and kinase domain.

(**C**) Interspecies coevolution plot (using patristic distance) between fungal Dip2 and PKC using three different phylogenetic algorithms, with the correlation coefficient value represented by r. Number of organisms and significance levels are indicated.

**(D)** Interspecies correlation coefficient values (r) for Dip2 compared with PKC and control proteins Gapdh and Pgk using various algorithms for calculating phylogenetic distances. r value is calculated for Gapdh and Pgk the same way. The table contains the exact correlation coefficient values for all the above-mentioned protein pairs using different algorithms.

(**E**) Coevolution analysis (using genetic distance) between Dip2 and PKC along with their individual comparison with control protein Gapdh. Number of organisms and significance levels are indicated.

(**F**) Correlation coefficient values represented as bar graph for Dip2 compared with a set of housekeeping genes and lipid metabolizing proteins.

The online version of this article includes the following source data and figure supplement(s) for figure 4:

**Figure 5 - Source data 1- 5C:** Quantification of interspecies correlation coefficient values for Dip2 and PKC using different algorithms.

**Figure 5 - Source data 2- 5D:** Quantification of interspecies correlation coefficient values for Dip2, PKC, Gapdh, and Pgk1 using different algorithms.

**Figure 5 - Source data 3- 5E:** Quantification of interspecies correlation coefficient values using genetic distances for Dip2, PKC and Gapdh.

**Figure 5 - Source data 4- 5F:** Quantification of interspecies correlation coefficient values for various housekeeping proteins and Dip2.

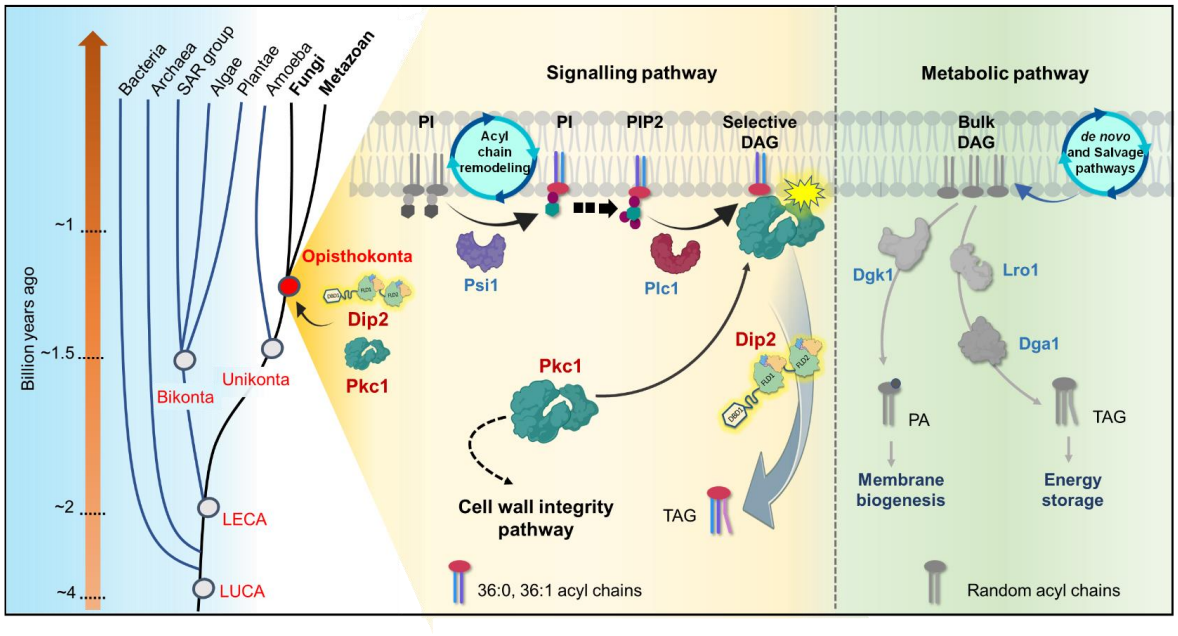


**Figure 6. A graphical representation depicting the emergence of Dip2-PKC axis and the evolution of selective DAG-based PKC signalling in Opisthokonta.**

Dip2 is recruited parallel to PKC in the tree of life at the root of Opisthokonta evolution ~1.2 billion years ago. This Dip2-PKC axis remains conserved across Fungi and Metazoan. Two distinct DAG pools are sourced from *de novo* or salvage pathways and acyl chain remodelling of PIs, leading to metabolic and signalling DAG pool, respectively. Remodelled phosphoinositides (PI, PIP, PIP2) by Psi1 are enriched with 18:0 acyl chains and channelled to corresponding PIP2, which forms respective DAG species (C36:0, C36:1) upon hydrolysis by Plc1. These selective DAG subspecies act as secondary messenger for PKC signalling and therefore regulate the CWI pathway in yeast. Dip2 maintains the levels of these selective DAGs by facilitating their conversion to TAGs, thereby creating a diversification of DAG function into metabolic and signalling pathways.

**Supplementary Figures:**

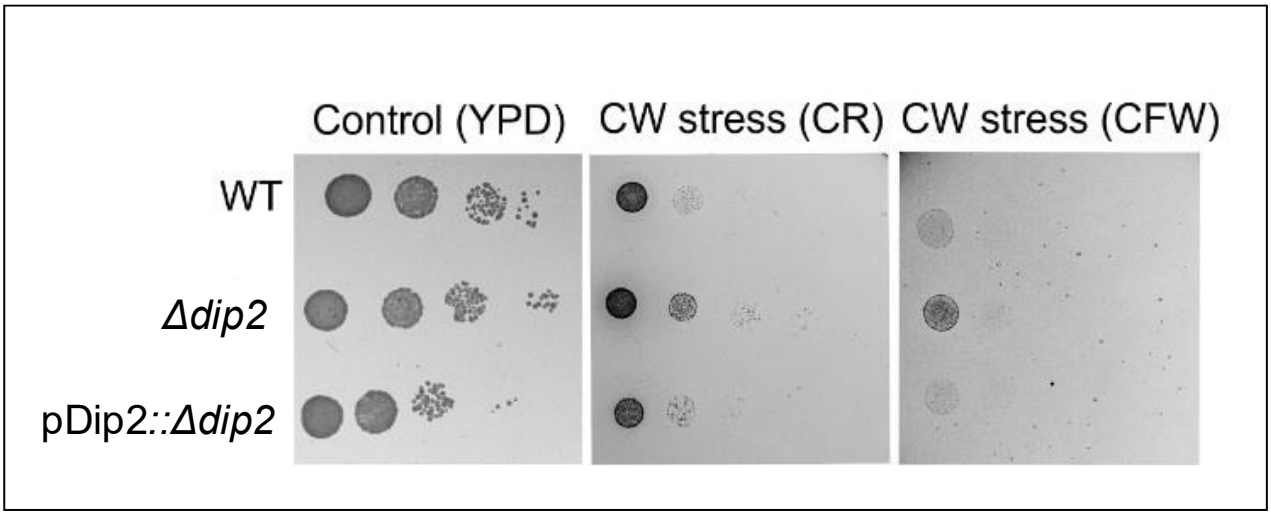


**Figure 1. figure supplement 1**

Serial dilution assay in YPD media for WT, *Δdip2*, pDip2::*Δdip2* represents *Δdip2* complemented with Dip2 expressed under its native promoter. Control plate contains YPD media and cell wall (CW) stress plate has either congo red (CR) (100µg/mL) or calcofluor white (CFW) (50µg/mL). N=3.

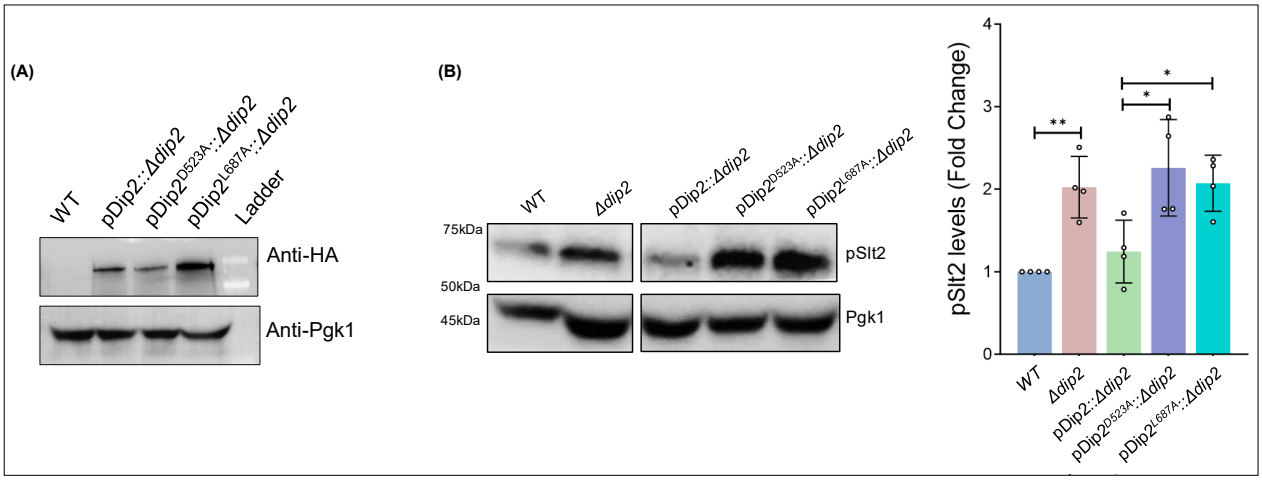


**Figure 1. figure supplement 2**

**(A)** Western blot image showing expression of wildtype Dip2-GFP-His-HA (219 kDa) and mutant Dip2 expressed in *Δdip2*. *WT* serves as a negative control and Pgk1(45 kDa) blot serves as the loading control.

**(B)** Representative western blot image showing pSlt2 (56 kDa) levels on complementing *Δdip2* with wildtype and catalytic mutant Dip2 ($Dip2^{D523A}$ and $Dip2^{L687A}$). Quantification of pSlt2 levels for *WT* and mutant Dip2 complemented *Δdip2* strain, normalised with total Slt2. Phosphoglycerate kinase (Pgk1) (45 kDa) has been used as a loading control. Data are represented as mean ± SD (unpaired, two-tailed Student's t-test; $N$=3; *p < 0.05; ns = not significant).

**Figure 1. figure supplement 2B - Source data 1:** pSlt2 quantification for *Δdip2* complemented by the catalytic mutants of Dip2.

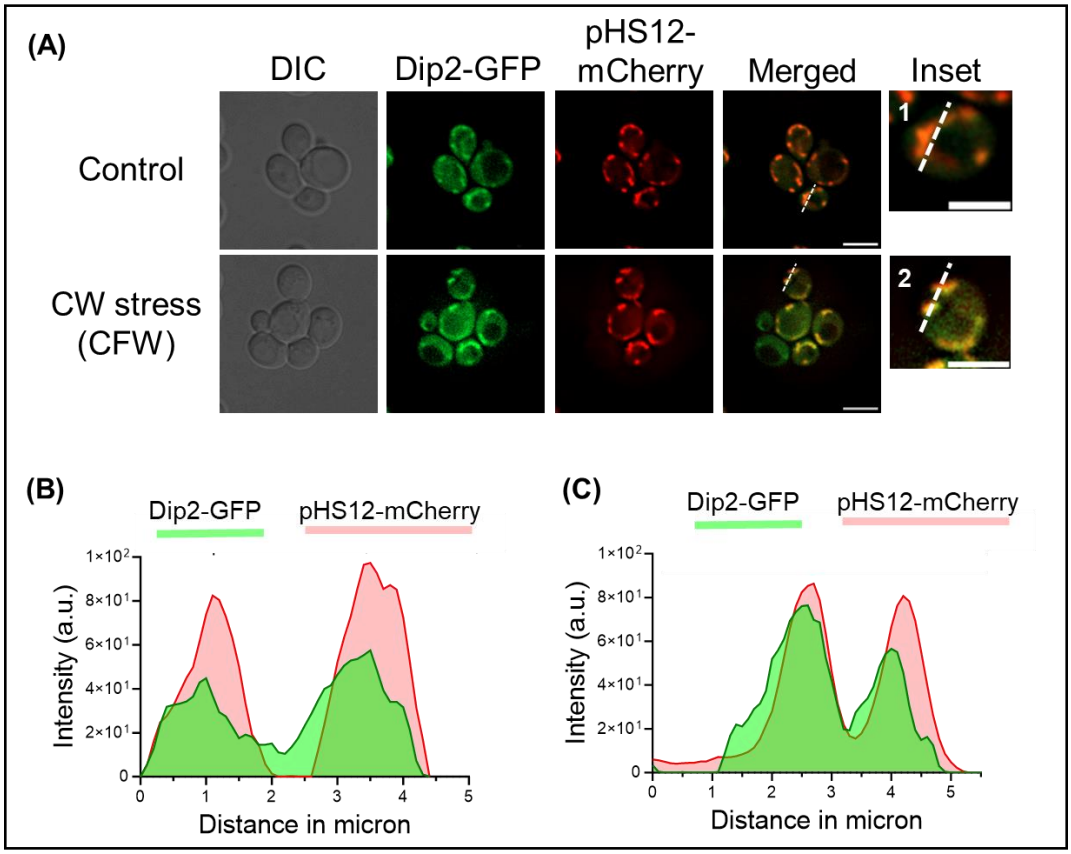


**Figure. 1. figure supplement 3**

**(A)** Microscopy image showing *WT* cells under normal condition (upper panel) and treated with calcofluor white (50µg/mL) (lower panel). Endogenous Dip2 has been tagged with

GFP, while mitochondria have been visualized by using a mitochondria-targeted mCherry plasmid transformed in Dip2-GFP cells. The enlarged images of representative bud cells for control and treated, marked with 1 and 2 respectively are shown in inset. Scale bar = 5µm.

**(B-C)** Line scan of signal intensity along the white line shown in inset images of (A), marked 1 and 2, respectively.

**Figure 1. figure supplement 3B - Source data 1**: Line scan intensity quantification for GFP and mCherry in Dip2-GFP control

**Figure 1. figure supplement 3C- Source data 2**: Line scan intensity quantification for GFP and mCherry in Dip2-GFP CFW treated.

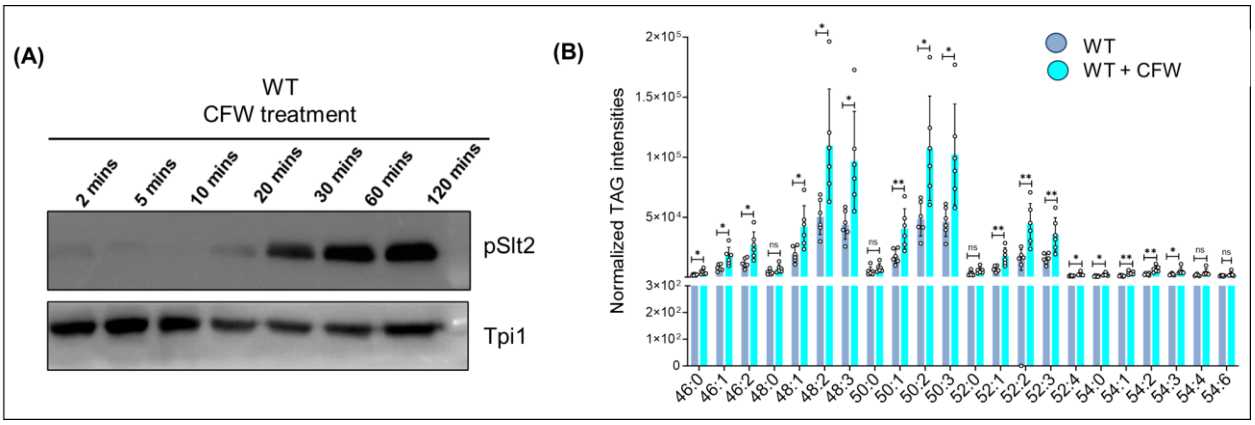


**Figure 2. figure supplement 1**

**(A)** Representative western blot showing increasing activation of Pkc1 pathway (the level of pSlt2) in a time-dependent manner upon CFW treatment (50µg/mL). Tpi1 (27 kDa) has been used as a loading control.

**(B)** Lipidomic quantification of TAGs for *WT* cells under cell wall stress in the presence of CFW (50µg/mL) compared to *WT* under normal growth condition.

**Figure 2. figure supplement 1B - Source data 1**: TAG quantification for WT and WT treated with CFW.

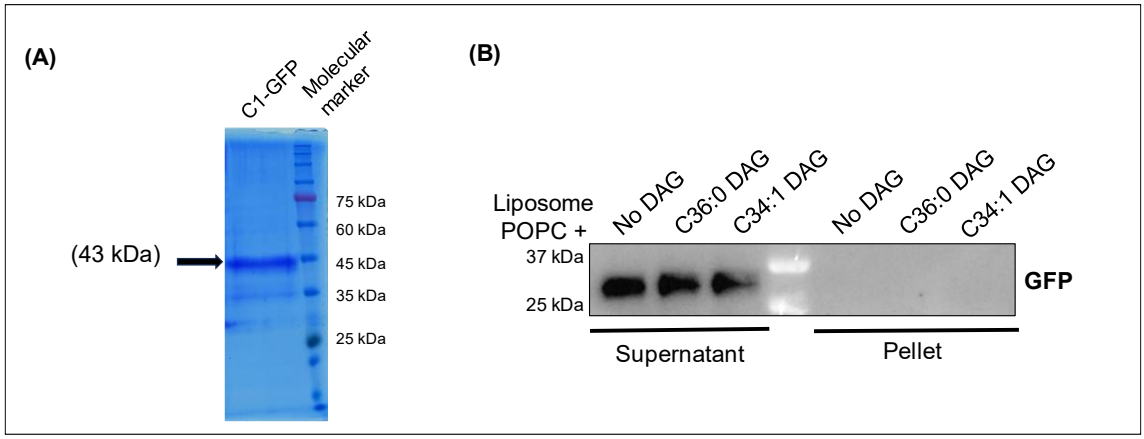


**Figure 2. figure supplement 2**

**(A)** Coomassie stained SDS-PAGE gel image of purified Pkc1-C1 domain, expressed and purified from yeast.

**(B)** Western blot showing no binding (in the pellet fraction) in case of incubation of liposomes with only GFP as a negative control.

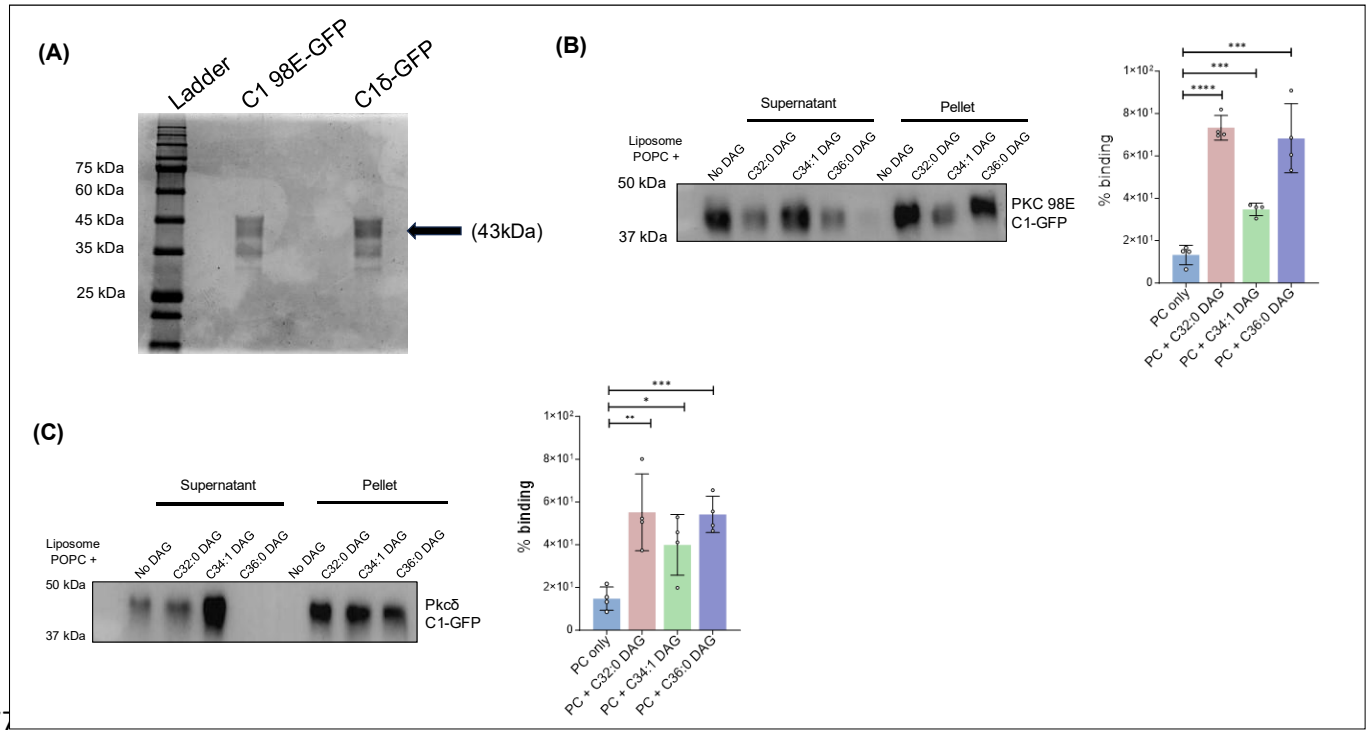


**Figure 2. figure supplement 3**

**(A)** SDS-PAGE gel stained with Coomassie showing purified C1 domain of *Drosophila melanogaster* (C198E-GFP) and *Rattus novergicus* (C1δ-GFP).

**(B)** Liposome binding assay for Pkc98E C1 domain from *Drosophila melanogaster* for multiple DAGs, probed using anti-GFP antibody. Bar graph showing the percentage of DAG binding of Pkc98E C1 domain for different DAG subspecies.

**(C)** Liposome binding assay for Pkcδ C1 domain from *Rattus novergicus* for multiple DAGs, probed using anti-GFP antibody. Bar graph showing the percentage of DAG binding of Pkcδ C1 domain for different DAG subspecies.

**Figure 2. figure supplement 3 - Source data 2**: Quantification for percent binding of Pkc98E and Pkcδ C1 domain with different DAG containing liposomes.

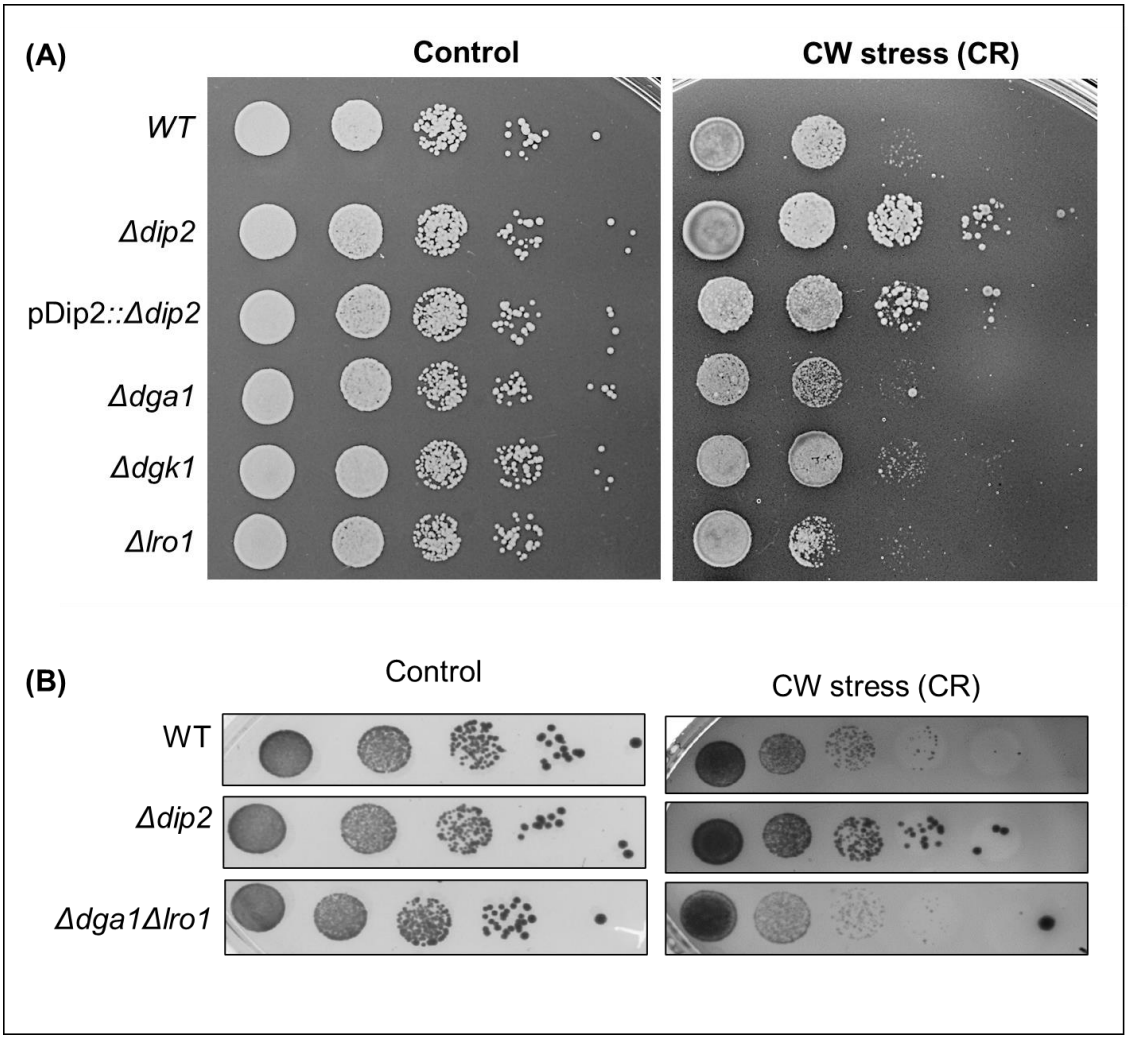


**Figure 3. figure supplement 1**

(A) Serial dilution assay for single deletions of DAG acting enzyme genes (*DGA1*, *LRO1* and *DGK1)* in the presence of CR (100µg/ml)**.** N=3.

(B) Serial dilution assay for the cell wall stress sensitivity *of Δdga1Δlro1*, compared to *WT* and Δ*dip2*, in the presence of CR (100µg/mL), compared to SC media control plate. N=3. SC media control image is same as that of Fig 3G.

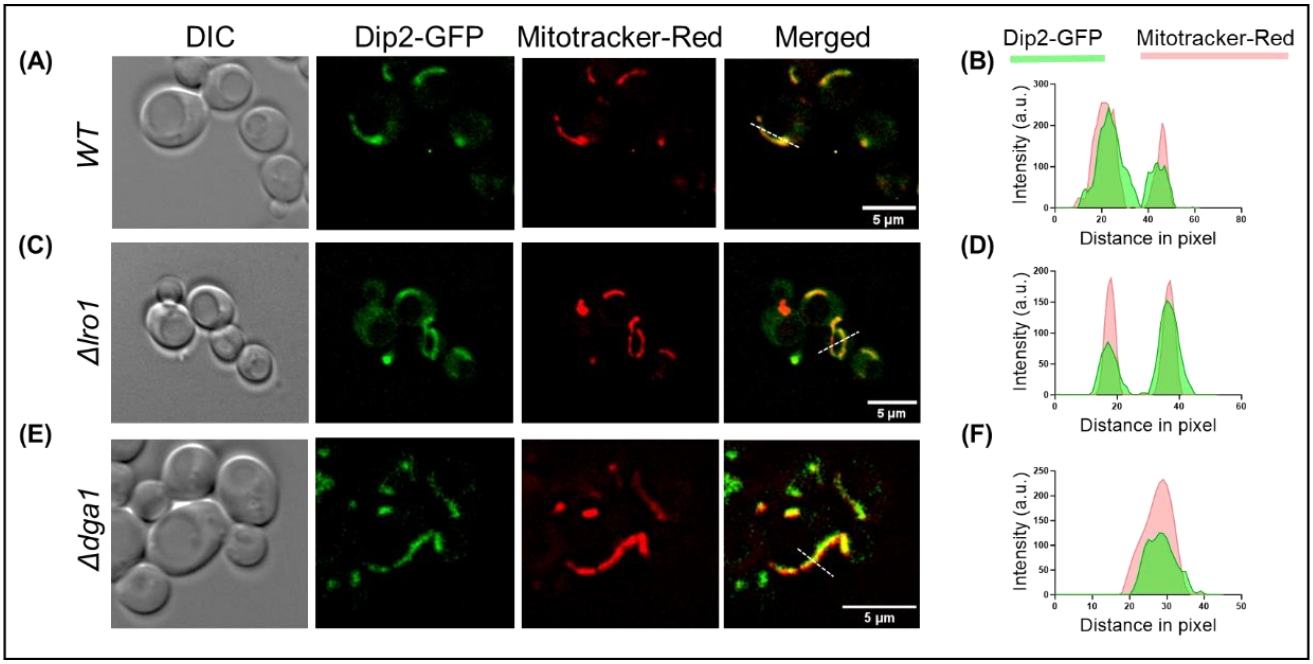


**Figure 3. figure supplement 2**

Live cell microscopy images showing the DIC images (left), Dip2 tagged with GFP (green), Mitotracker Red (red) and merged images for red and green channels (right) for **(A)** *WT*, **(C)** *Δlro1* and **(E)** *Δdga1*. Scale bar represents 5 µm.

Line scan of signal intensity along the white lines shown in the respective merged images of **(B)** *WT*, **(D)** *Δlro1* and **(F)** *Δdga1*. Green and red peaks represent Dip2-GFP and mitotracker red, respectively.

**Figure 3. figure supplement 2B - Source data 1**: Line scan intensity quantification for Dip2-GFP and MitoTracker Red in WT control.

**Figure 3. figure supplement 3D- Source data 2**: Line scan intensity quantification for Dip2-GFP and MitoTracker Red in *Δlro1*.

**Figure 3. figure supplement 3F- Source data 3**: Line scan intensity quantification for Dip2-GFP and MitoTracker Red in *Δdga1*.

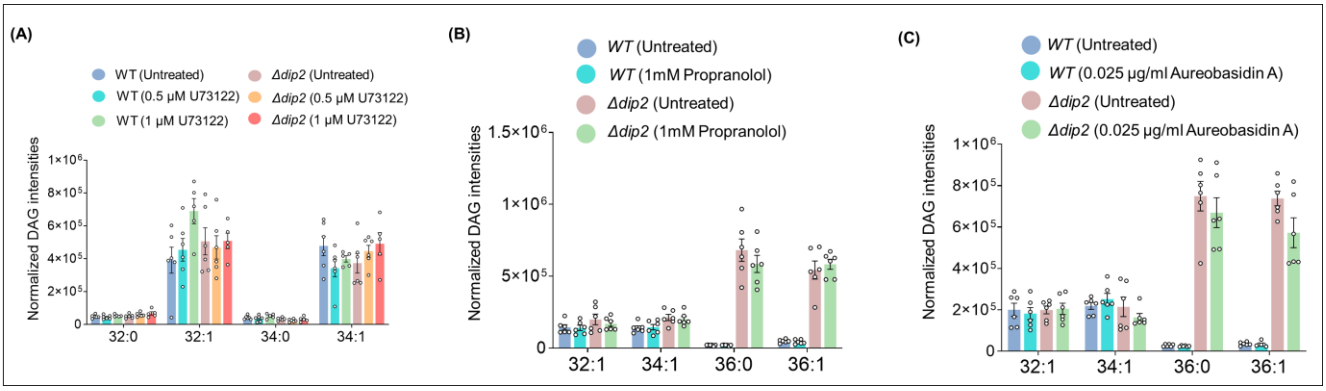


**Figure 4. figure supplement 1**

**(A)** Lipidomic analysis showing the levels of bulk DAGs in WT and *Δdip2* on treating with 0.5 and 1 μM of U73122. Data are represented as mean ± SEM (unpaired, two- tailed Student's t-test). N = 6.

**(B)** Lipidomic analysis for the DAG subspecies in *WT* and *Δdip2* in the presence and absence of Propranolol and **(C)** Aureobasidin. Data are represented as mean ± SEM (unpaired, two-tailed Student's t-test; ns = not significant). N = 6.

**Figure 4. figure supplement 1A- Source data 1**: DAG quantification for WT and *Δdip2* treated with U73122.

**Figure 4. figure supplement 1B- Source data 2**: DAG quantification for WT and *Δdip2* treated with propranolol.

**Figure 4. figure supplement 1C- Source data 3**: DAG quantification for WT and *Δdip2* treated with aureobasidinA.

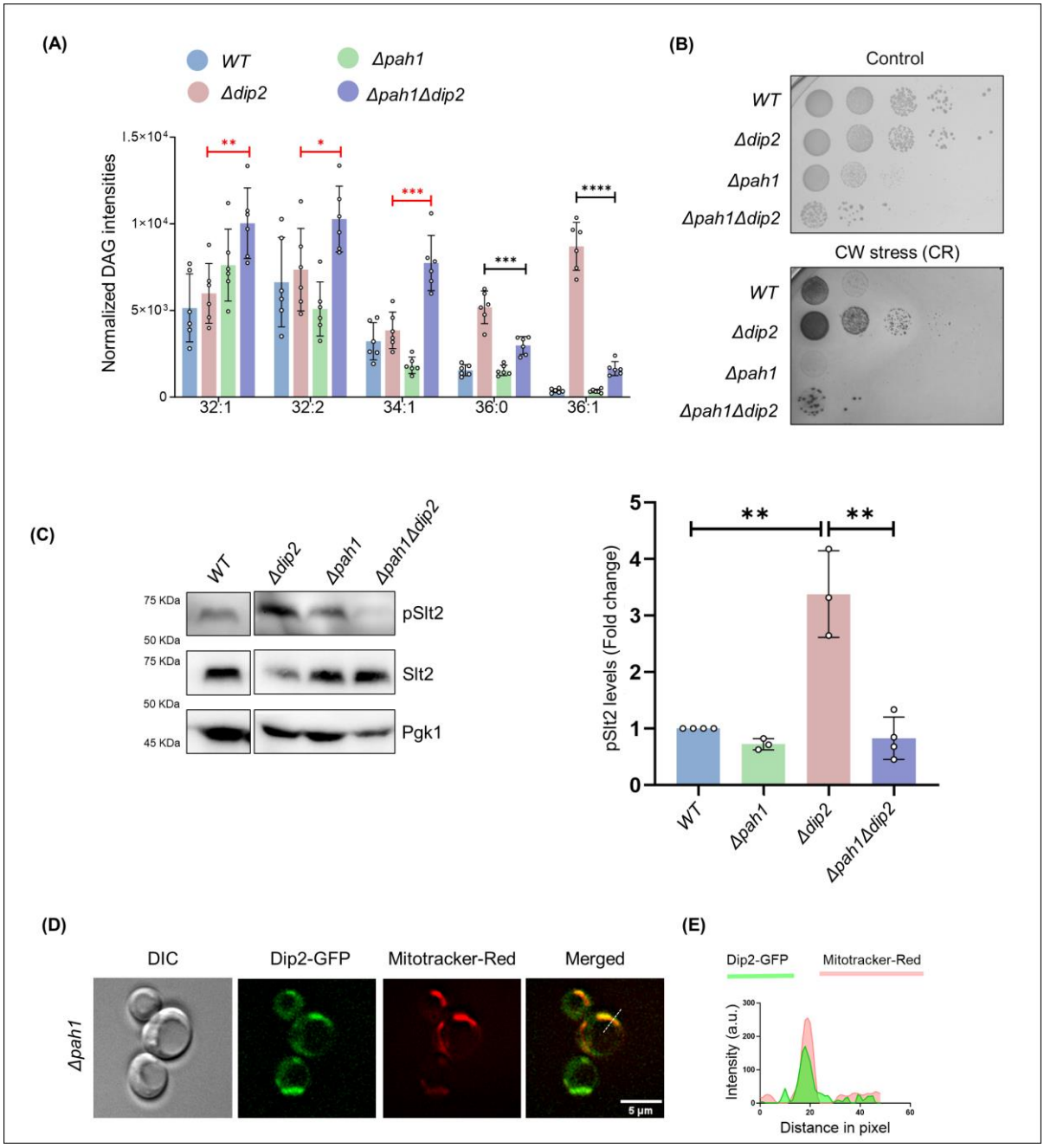


**Figure 4. figure supplement 2**

**(A)** Bar graph showing quantification of DAG subspecies level in *Δpah1* and *Δpah1Δdip2* DKO. Significance in red shows increase in DAG species while the black arrows show decrease in DAGs. Data are represented as mean ± SEM (unpaired, two-tailed Student's t-test; n = 6). ****p < 0.0001; ***p < 0.001 ns = not significant. N=6.

**(B)** Cell wall stress assay for Δ*pah1* and Δ*pah1Δdip2*, compared with *Δdip2,* in the presence of congo red (100µg/mL).

**(C)** Western blot and quantification of pSlt2 (56 kDa) in Δ*pah1* and Δ*pah1Δdip2*, normalized to total Slt2 (56 kDa). Pgk1 (45 kDa) is used as a loading control. Data are represented as mean ± SD (unpaired, two-tailed Student's t-test; *n*=3; **p < 0.01; ns = not significant).

**(D)** Live cell microscopy image for Dip2-GFP in *Δpah1* co-stained with Mitotracker Red (red). Scale bar represents 5 µm.

**(E)** Line scan of signal intensity along the white line shown in the merged image. Green and red peaks represent Dip2-GFP and mitotracker red, respectively.

**Figure 4. figure supplement 2A- Source data 4**: DAG quantification for *Δpah1 and Δpah1Δdip2*.

**Figure 4. figure supplement 2C- Source data 5**: pSlt2 quantification for *Δpah1 and Δpah1Δdip2*.

**Figure 4. figure supplement 2E- Source data 6**: Line scan intensity quantification for Dip2-GFP and MitoTracker Red in *Δpah1.*

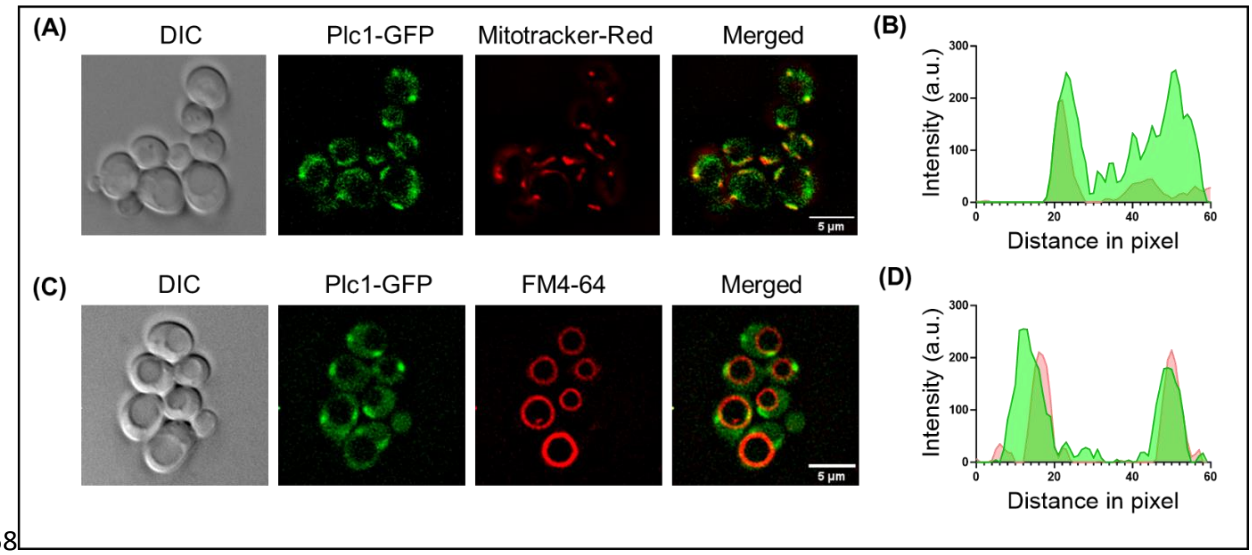


**Figure 4. figure supplement 3**

**(A)** Microscopy image panel showing DIC image (left), fluorescence for Plc1 tagged with GFP, mitotracker-red for staining mitochondria and the merged image for both the fluorophores (right). Scale bar represents 5 µm.

**(B)** Line scan plotted for the fluorescence intensity of Plc1-GFP along with mitotracker-red across the line shown in the merged panel.

**(C)** Microscopy image panel for Plc1-GFP stained with FM4-64 for visualizing vacuoles. Th merged image for red and green channel is sown on the right. Scale bar represents 5 µm.

**(D)** Fluorescence intensity plotted for GFP and FM4-64 along the line showing colocalization of Plc1 with vacuole.

**Figure 4. figure supplement 3B- Source data 7**: Line scan intensity quantification for Plc1-GFP and MitoTracker Red.

**Figure 4. figure supplement 3D- Source data 8**: Line scan intensity quantification for Plc1-GFP and FM4-64.

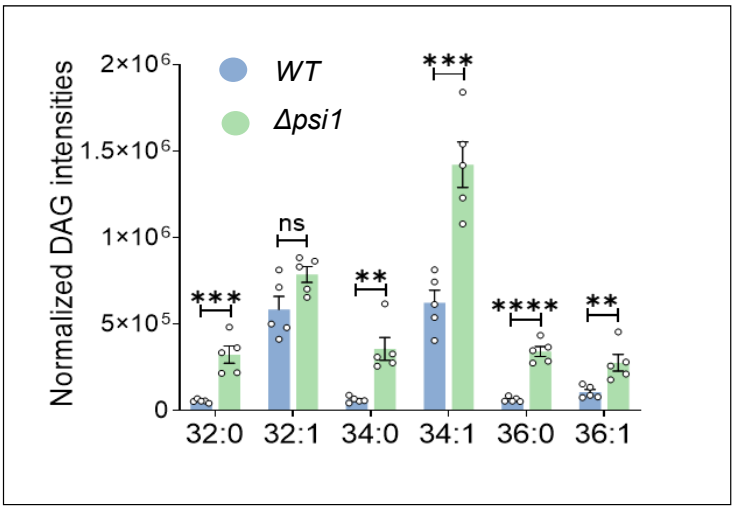


**Figure 4. figure supplement 4**

DAG subspecies quantification for *Δpsi1* measured via lipidomics. Data are represented as mean ± SEM (unpaired, two-tailed Student's t-test; N=5). ****p < 0.0001; ***p < 0.001, **p < 0.01, ns = not significant.

**Figure 4. figure supplement 4- Source data 9**: DAG quantification for *Δpsi1*.

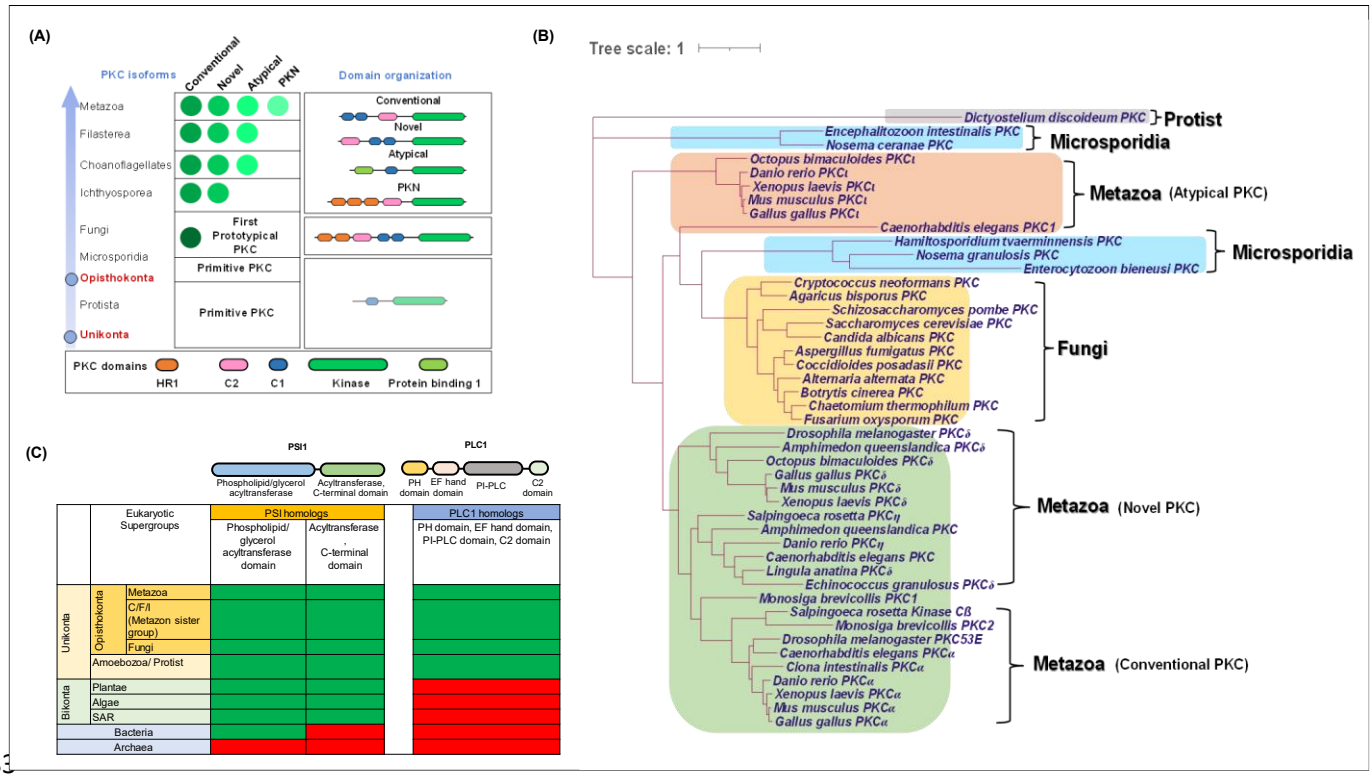


## Figure 5. figure supplement 1

**(A)** A schematic showing domain architecture and distribution of PKC isoforms (green circles) across Unikonta. Further classification of PKC isoforms (conventional, novel, atypical and Protein Kinase C-Related Kinase (PKN)) and domain annotations are indicated.

**(B)** Phylogenetic profiling of PKC showing its distribution among protists (grey), microsporidia (blue), fungi (yellow) and metazoan (green). Types of PKC isoforms found in metazoan are mentioned in bracket.

**(C)** Distribution of Psi1 and Plc1 and their domains across tree of life. Domain organizations of both Psi1 and Plc1 are shown on the top. Green and red colours represent the presence and absence of the proteins in respective supergroups mentioned on the left side.

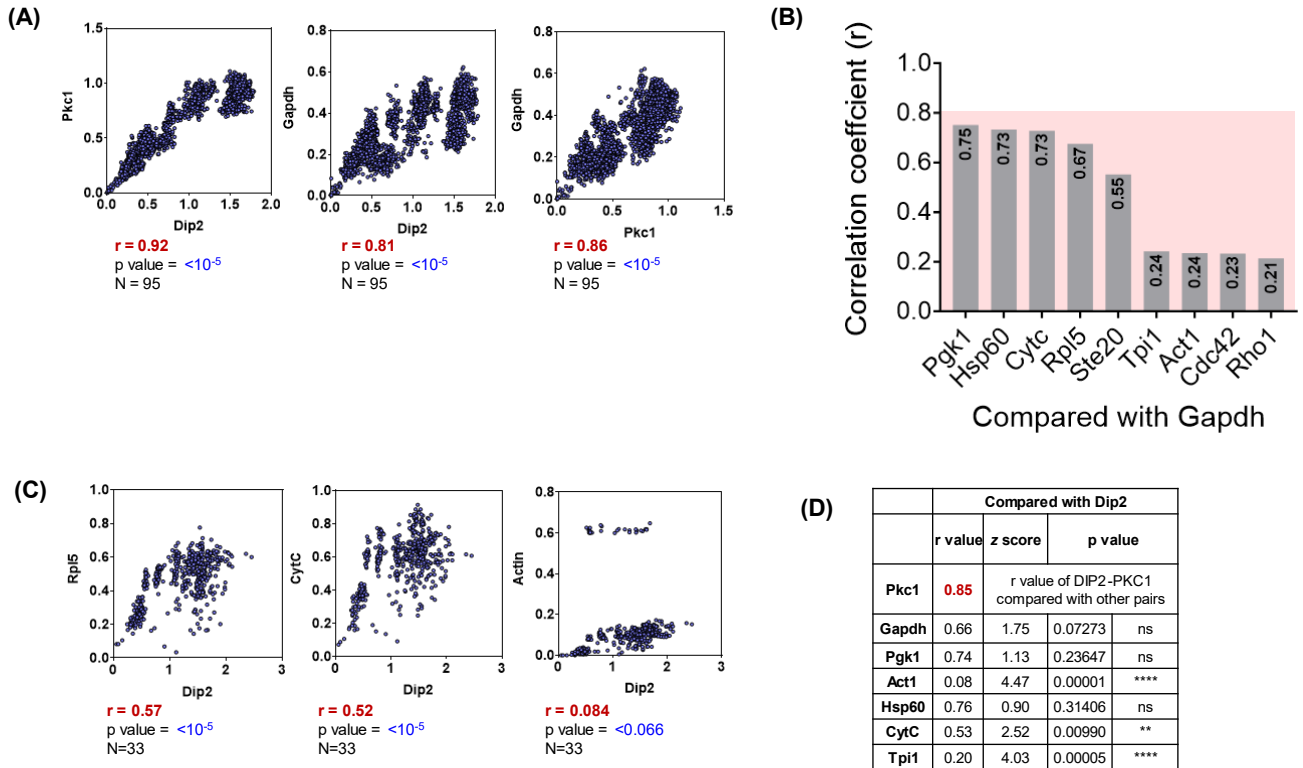


(D)

| | Compared with Dip2 | | | |
|---|---|---|---|---|
| | r value | z score | p value | |
| Pkc1 | 0.85 | r value of DIP2-PKC1 compared with other pairs | | |
| Gapdh | 0.66 | 1.75 | 0.07273 | ns |
| Pgk1 | 0.74 | 1.13 | 0.23647 | ns |
| Act1 | 0.08 | 4.47 | 0.00001 | **** |
| Hsp60 | 0.76 | 0.90 | 0.31406 | ns |
| CytC | 0.53 | 2.52 | 0.00990 | ** |
| Tpi1 | 0.20 | 4.03 | 0.00005 | **** |
| Cdc42 | 0.13 | 4.30 | 0.00001 | **** |
| Rho1 | 0.33 | 3.48 | 0.00040 | *** |
| Ste20 | 0.50 | 2.65 | 0.00619 | ** |
| Rpl5 | 0.57 | 2.26 | 0.01841 | * |
| Tgl3 | 0.39 | 3.21 | 0.00108 | ** |
| Erg4 | 0.57 | 2.31 | 0.01841 | * |
| Faa1 | 0.64 | 1.85 | 0.05377 | ns |
| Lcb1 | 0.25 | 3.81 | 0.00011 | *** |

**Figure 5. figure supplement 2**

**(A)** Interspecies correlation plot for Dip2 & Pkc1 and Gapdh with Pkc1 and Dip2 each from all the fungal sequences present in KEGG Genome Database.

**(B)** Correlation coefficient values represented as a bar graph for Gapdh compared to other protein controls. Pink colour window behind the bar graphs shows the empirical cut-off of 0.8 correlation coefficient.

**(C)** Interspecies correlation plot between Dip2 and various control proteins like Ribosomal 60s subunit protein L5 (Rpl5), Cytochrome C (CytC) and Actin.

**(D)** A table representing the correlation coefficient (r-value), Fisher's z-scores (z-score) and p-value for Dip2 compared with Pkc1 and other protein controls.

**Figure 5 - figure supplement 2A- Source data 1:** Quantification of interspecies correlation coefficient values for Dip, PKC and Gapdh control for all fungal species.

**Figure 5 - figure supplement 2B- Source data 2:** Quantification of interspecies correlation coefficient values for various housekeeping proteins with Gapdh.

**Figure 5 - figure supplement 2C- Source data 3:** Quantification of interspecies correlation coefficient values for Dip compared with Rpl5, CytC and Actin.

**Figure 5 - figure supplement 2D- Source data 4:** Quantification of interspecies correlation coefficient values, Fisher's z-scores (z-score) and p-value for Dip2 compared with Pkc1 and other protein control.